EurJIC
European Journal of Inorganic Chemistry

Full Papers
doi.org/10.1002/ejic.202100109

Chemistry Europe
European Chemical Societies Publishing

Two-Photon Absorption Properties in "Push-Pull" Ruthenium Nitrosyl Complexes with various Fluorenylterpyridine-Based Ligands

Valerii Bukhanko,[a] Andrés Felipe León-Rojas,[b] Pascal G. Lacroix,*[a] Marine Tassé,[a] Gabriel Ramos-Ortiz,[c] Rodrigo M. Barba-Barba,[c] Norberto Farfán,[b] Rosa Santillan,[d] and Isabelle Malfant*[a]

Using the compound $[Ru^{II}(FT)(bipy)(NO)](PF_6)_3$ (FT is the electron-rich 4′-(2-fluorenyl)-2,2′:6′,2″-terpyridine ligand and bipy is 2–2′bipyridine) as a reference, two new compounds are presented in which carbon-carbon double and triple bonds are inserted between the fluorenyl substituent and the terpyridine to provide an extended conjugation path. The electronic properties of the three complexes are compared experimentally by UV-visible spectroscopy and computationally by means of the density functional theory. All of them exhibit a capability for NO release under irradiation on their low-energy transition located in the 400–500 nm range, with a quantum yield around 0.01. Their two-photon absorption (TPA) cross sections are investigated by the Z-scan technique at $\lambda = 800$ nm. While the reference compound exhibits a cross-section equal to 108 GM, the introduction of double and triple bonds leads to increased cross-sections equal to 131 GM and 150 GM, respectively. These values are discussed in reference to the two-level model in use for "push-pull" dipolar TPA chromophores.

Introduction

Since it was identified as the endothelium-derived relaxing factor by Ignarro and Palmer, in 1987,[1,2] nitric oxide ($NO^{\bullet}$) has been attracting a growing interest in relation to its increasingly recognized biological functions and possible therapeutic applications.[3,4] However, the action of $NO^{\bullet}$ in biological media may strongly depend on its concentration. For instance, at micromolar concentration, it acts as a potential anticancer agent, promoting apoptosis and inhibiting angiogenesis, whereas lower concentrations promote cells growth with application for tissue healing.[5–7] In this context, exogenous $NO^{\bullet}$ donors have been widely investigated,[8] but they must be able to deliver $NO^{\bullet}$ locally and quantitatively to avoid undesirable effect on untargeted cells. Among various potential candidates, ruthenium nitrosyl complexes have emerged as an appealing class of biological materials in relation to their low toxicity, good stability, and moreover to their capability to exclusively release $NO^{\bullet}$ under irradiation in the $\lambda = 300$–500 nm domain, taking advantage of the non-invasive and highly controllable characteristics of light.[9–11] Nevertheless, and in order to be fully applicable, the irradiation should be achieved in the $\lambda = 600$—1 300 nm "therapeutic window" of relative transparency of the biological media.[12]

To design alternative $NO^{\bullet}$ donors, compatible with the therapeutic window, we have previously reported on a Ru(NO) complex built up with fluorenylterpyridine and a bipyridine ligand ($\mathbf{1}^{3+}$, in Scheme 1).[13] Introducing a fluorene substituent on the terpyridine was motivated by its well documented capability to enhance the two-photon absorption (TPA) properties of molecules.[14] In the last decade, the TPA technique which involves two photons at double wavelength of the one-photon excitations (*e.g.* $\lambda = 800$ nm instead of 400 nm) has emerged as the most promising technic in the photo-dynamic therapy (PDT) treatment of cancer, microsurgery, local drug delivery and high resolution cell imaging.[15,16] These enhanced capabilities are related to its low damage effects, high selectivity and deeper penetration into biological tissues. Along this line, the factor of merit of $NO^{\bullet}$ donors is an uncaging parameter arising as the product of the release efficiency ϕ_{NO} (number of $NO^{\bullet}$ generated per $NO^{\bullet}$ donors promoted in the excited state) by the TPA capability of the $NO^{\bullet}$ donors, known as the TPA cross-section (σ_{TPA}). Therefore, any attempt to enhance the capability of Ru(NO) complexes will imply increasing either ϕ_{NO} or σ_{TPA}. In $\mathbf{1}^{3+}$, ϕ_{NO} lies around 0.01, a value that appears satisfactory. Indeed, increasing ϕ_{NO} significantly complicates the handling of the species, since a short exposition to light initiates the decomposition of the complex with the outcome of potential undesirable $NO^{\bullet}$ effect on healthy tissues. On the other hand, the TPA cross section of $\mathbf{1}^{3+}$ is equal to 108.0 ± 18.0 GM at 800 nm, far below values determined for large size poly-

[a] Dr. V. Bukhanko, Dr. P. G. Lacroix, M. Tassé, Prof. I. Malfant
CNRS, Laboratoire de Chimie de Coordination (LCC),
205 route de Narbonne, 31077 Toulouse, France
E-mail: pascal.lacroix@lcc-toulouse.fr
isabelle.malfant@lcc-toulouse.fr
[b] A. F. León-Rojas, Dr. N. Farfán
Facultad de Química, Departamento de Química Orgánica, Universidad Nacional Autónoma de México, 04510 CDMX., México
[c] Dr. G. Ramos-Ortiz, Dr. R. M. Barba-Barba
Centro de Investigaciones en Óptica,
A.P. 1–948, 37000 León, México
[d] Dr. R. Santillan
Departamento de Química,
Centro de Investigación y de Estudios Avanzados del IPN,
07000, A.P. 14–740, Ciudad de México, México

Supporting information for this article is available on the WWW under https://doi.org/10.1002/ejic.202100109

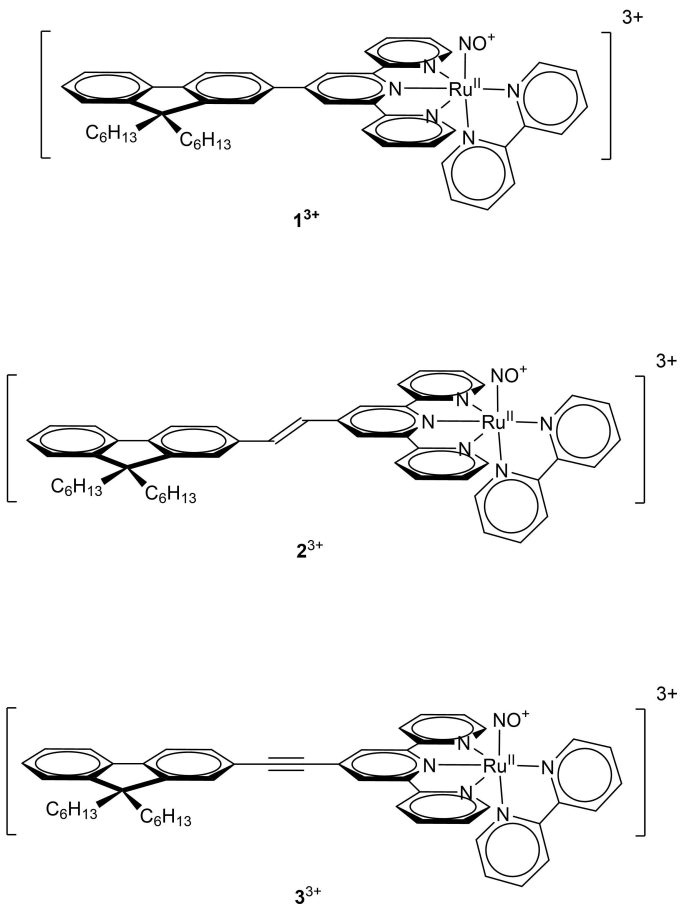

Scheme 1. Ruthenium nitrosyl complexes under investigation

ruthenium-based dendrimers specially designed to target record cross-sections (higher than 10 000 GM).[17] These observations encouraged us to direct our research effort towards an increase of σ_{TPA} by chemical modifications achieved on the $\mathbf{1}^{3+}$ complex.

The present contribution is devoted to the investigation of alternative ruthenium nitrosyl complexes with enhanced TPA capability, within the dipolar approach previously used in $\mathbf{1}^{3+}$. Owing to the comprehensive analysis on the origin of TPA effects in molecules, which relates the properties to long range charge transfer transitions,[15,16,18] the selected strategy aims at the insertion of a –CH=CH– double and a –C≡C– triple bonds between the fluorenyl unit and the terpyridine, thus leading to complexes $\mathbf{2}^{3+}$ and $\mathbf{3}^{3+}$, respectively (Scheme 1). After describing the synthesis and characterization of the new species, their spectroscopic and TPA properties are presented and compared with those of the parent $\mathbf{1}^{3+}$ species. The differences are analyzed computationally within the framework of the time-dependent density functional theory (TD-DFT) to evaluate the capacities of extended π-delocalization to enhance the charge transfer effects and hence the TPA response of these ruthenium nitrosyl derivatives.

Results and Discussion

Synthesis and characterization

The synthetic routes towards substituted terpyridine ligands **A** and **B** used in the synthesis of complexes $\mathbf{2}^{3+}$ and $\mathbf{3}^{3+}$, respectively, are described in Scheme 2. Ligand **A** was obtained through a 6 steps linear type synthesis. In a first step, the fluorene moiety was modified by insertion of two hexyl chains, to substantially improve the solubility of the final complex. This approach was described in previous papers: high solubility of complexes (around 10^{-2} M) was crucial for measuring TPA response of the complexes.[13] The incorporation of a double bond into the structure was addressed through a Heck-type coupling of **2a** with methylacrylate, similarly to the procedure described in the literature for analogous compounds.[19] The resulting ester **2b** was further converted to the corresponding aldehyde **2d** through reduction of **2b** and subsequent oxidation of the acrylic alcohol **2c**. Two succeeding steps, Claisen condensation with 2-acetylpyridine and Michael reaction of the obtained chalcone **2e** with Kröhnke salt in the presence of ammonium acetate resulted in the formation of the final terpyridine (**A**) core.

Ligand **B** was synthesized by a more convenient 7 steps convergent approach depicted in Scheme 2. Thus, a triple bond was introduced into the structure through Sonogashira coupling of **2a** with TMS-protected acetylene, and subsequent deprotection of the acetylenic position resulted in formation of **3b**. The synthesis of the terpyridine core (**3e**) was achieved separately, following the procedure initially used by Constable and Ward and well-described in the literature.[20,21] The final step of the terpyridine synthesis consists on introduction of triflate group, which further enables Sonogashira coupling between compounds **3b** and **3e**, thus producing the desired ligand **B** with 42% yield. Applying a similar convergent approach to the synthesis of ligand **A**, with the only difference being introduction of a double bond instead of triple bond, was not successful due to the low yield of the final Heck-coupling step (1–2%). Therefore, an alternative linear way for the synthesis of ligand **A** was preferred.

The final compounds [**2**]$(PF_6)_3$ and [**3**]$(PF_6)_3$ were obtained by an approach previously used for the synthesis of bipyridine-terpyridine ruthenium-nitrosyl complexes.[13] The first step of complexes synthesis implies the reaction of ligands **A** or **B** with $RuCl_3$, which results in the formation of a paramagnetic complex [Ru(L)Cl_3] (Scheme 3). In a second step, [Ru(L)Cl_3] interacts with 2,2′-bipyridine in the presence of triethylamine to form the diamagnetic species [Ru(L)(bipy)Cl]Cl. Use of triethylamine facilitates the reduction of Ru^{III} to Ru^{II}. A subsequent ligand substitution provides a convenient approach to ruthenium-nitro complex [Ru(L)(bipy)NO_2]Cl, which is then converted to ruthenium-nitrosyl species [Ru(L)(bipy)NO]$(PF_6)_3$ upon treatment with concentrated HCl.

The formation of complexes [Ru(L)(bipy)NO_2]Cl and [Ru(L)(bipy)NO]$(PF_6)_3$ can be easily monitored by ^{1}H NMR spectroscopy. The proton in position 6 of bipyridine (Scheme 3) is spatially closed to the monodentate ligand present in the

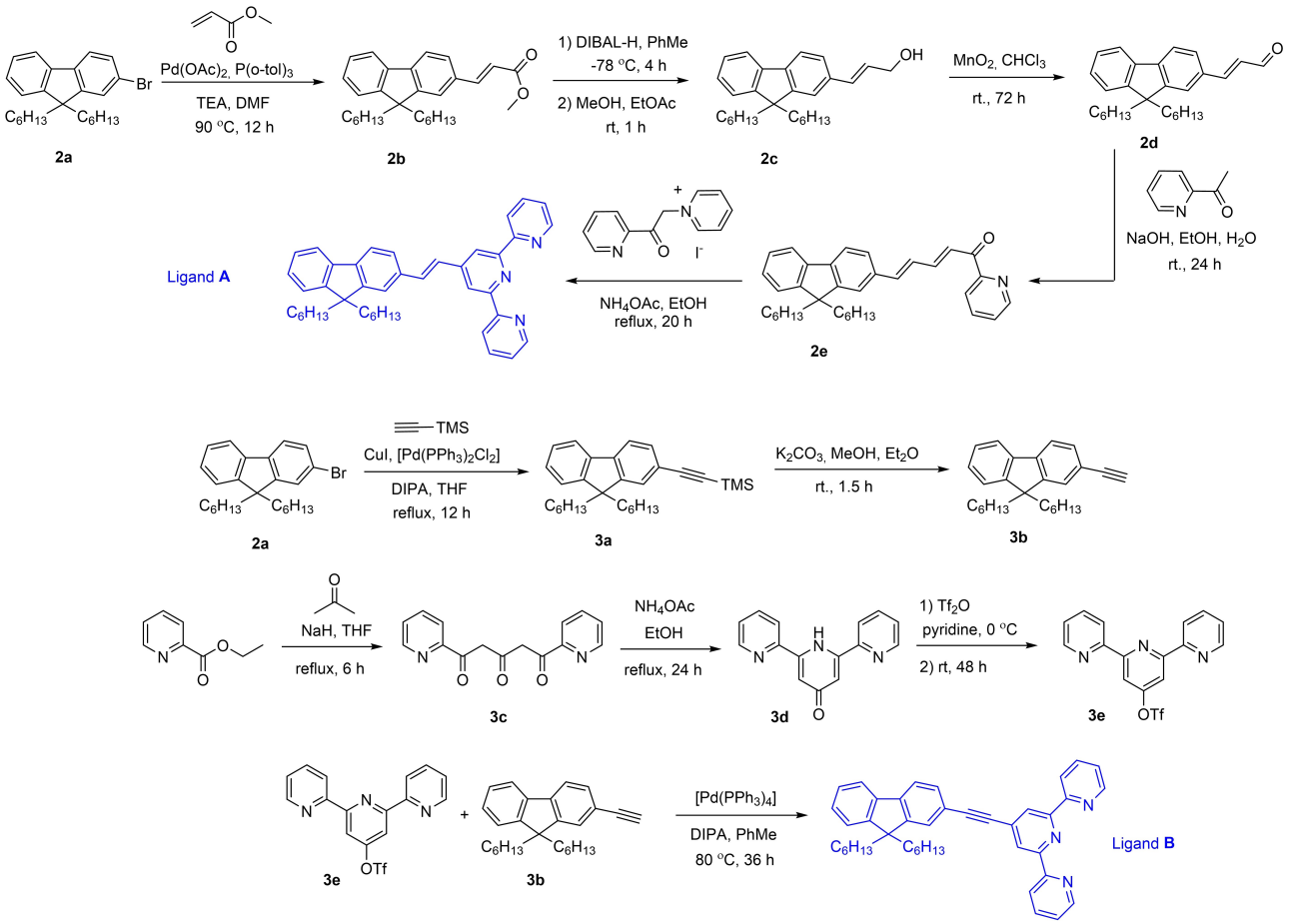

Scheme 2. Synthetic route towards Ligand **A** (top) and Ligand **B** (bottom).

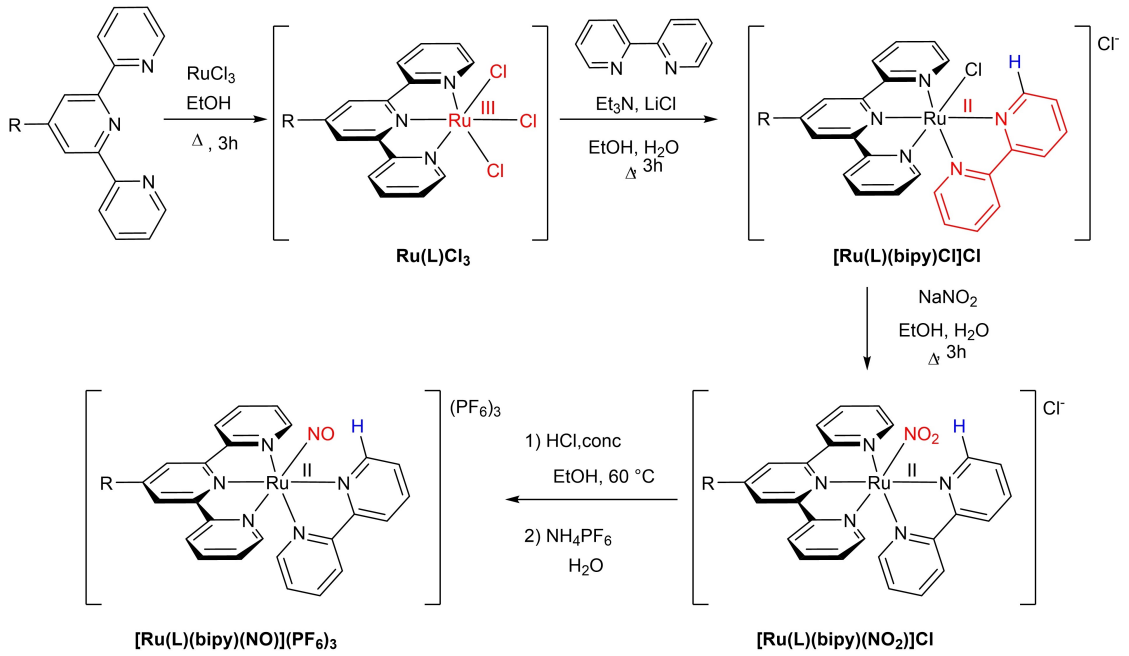

Scheme 3. Synthetic approach for the preparation of [**2**]$(PF_6)_3$ and [**3**]$(PF_6)_3$, built from ligands **A** and **B**, respectively. R stands for the fluorenyl-based substituents present in **A** and **B**. Hydrogen 6-H (in Blue) is used to monitor the Cl→NO_2→NO substitution, by ^{1}H-NMR.

complex. Its chemical shift in the ^{1}H-NMR spectra strongly depends on the nature of this ligand (Cl, NO_2, NO), as is illustrated in Figure 1, for the series of complexes leading to [**3**](PF$_6$)$_3$.

In the case of ruthenium complexes having a chlorido ligand in the coordination sphere, the chemical shift of the proton H(1) is 10.23 ppm (in CD_3OD), whereas for its nitro-analogue the peak of the proton H(1) is at 9.90 ppm (in CD_3OD). In the final ruthenium-nitrosyl complex [**3**](PF$_6$)$_3$ the peak of the corresponding proton is located at 9.31 ppm (in CD_3CN). The structures of both complexes [**2**](PF$_6$)$_3$ and [**3**](PF$_6$)$_3$ were confirmed by NMR, applying two-dimensional NMR-technics HMBC, HMQC and COSY.

The NO-bond stretching vibration frequencies are 1942 cm^{-1} and 1946 cm^{-1} for complexes [**2**](PF$_6$)$_3$ and [**3**](PF$_6$)$_3$, respectively. These values are very close to those previously reported by our group for similar complexes, containing five pyridine rings in coordination spheres of ruthenium atom.[13,22] These values indicate that the Ru-N–O moiety adopts a highly linear geometry, which is in a good agreement with previous observations.[22]

Spectroscopic Properties

The experimental UV-visible spectra of the three Ru(NO) complexes are shown in Figure 2. Contrary to their related substituted-terpyridine ligands, which possess bands with absorption maxima below 350 nm (Supplementary Materials), the complexes exhibit additional transitions at lower energy: an intense low energy band with absorption maxima around $\lambda =$ 450–500 nm (band 1), and a poorly resolved group of transitions in the $\lambda =$ 325–425 nm range (band 2). Intense transitions, reminiscent of those of the ligands are present below 350 nm (band 3), but will not be analyzed here. Interestingly, a clear red shift of 39 nm and 11 nm is observed at absorption maxima for the low-energy transitions on going from [**1**](PF$_6$)$_3$ to [**2**](PF$_6$)$_3$ and [**3**](PF$_6$)$_3$, respectively. The intensities of these transitions (extinction coefficients ε) are slightly enhanced in [**2**](PF$_6$)$_3$ and [**3**](PF$_6$)$_3$ versus that of the reference [**1**](PF$_6$)$_3$ (see Table 1). It is generally expected that both effects (excitations at longer wavelengths and enhanced intensities) lead to chromophores of better TPA capabilities.[23,24]

Table 1. Comparison between the experimental (UV-visible, acetonitrile) and the computed (TD-DFT) data for the low-lying transition in the three ruthenium complexes under investigations, with absorption maxima (λ_{max} in nm), extinction coefficients (ε in mol^{-1}.L.cm^{-1}), and oscillator strengths (f).

Compounds	UV-visible		TD-DFT	
	λ_{max}	ε	λ_{max}	f
[**1**](PF$_6$)$_3$	455	16 700	430	0.314
[**2**](PF$_6$)$_3$	494	25 100	484	0.802
[**3**](PF$_6$)$_3$	466	20 900	457	0.802

The TD-DFT computed spectra of the three complexes $\mathbf{1}^{3+}$, $\mathbf{2}^{3+}$ and $\mathbf{3}^{3+}$ are shown in Figure 3. The main difference versus experiment is observed at the intermediate band 2 (325–425 nm range), which appears well resolved by DFT, and spread into several overlapping components in the UV-visible spectra. Nevertheless, the low-energy bands of absorption are well defined, and related to a single high intensity transition. The data are gathered in Table 1 for these transitions, to be compared to the experimental data. The agreement between computation and experiment appears satisfactory. In particular, the maximum energy difference is limited to 0.16 eV in the worst case ([**1**](PF$_6$)$_3$), which is excellent for chromophores having long range charge transfer capacities.[25] Moreover, the trends observed in red shifts and changes in transition intensities are qualitatively reproduced by DFT. Altogether, these features allow us to use the computation to provide a precise analysis of the origin of the transitions at the orbital level (Table 2).

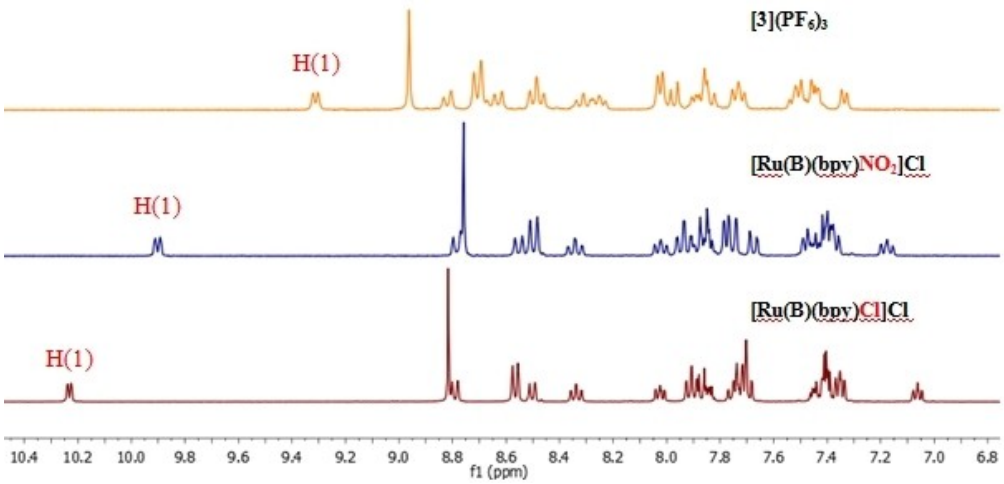

Figure 1. Change in ^{1}H-NMR-spectra upon substitution of monodentate ligand in the synthesis of complex [**3**](PF$_6$)$_3$. Spectra of [Ru(**B**)(bipy)NO$_2$]Cl and [Ru(**B**)(bipy)Cl]Cl were measured in CD_3OD, spectrum of [**3**](PF$_6$)$_3$ in CD_3CN.

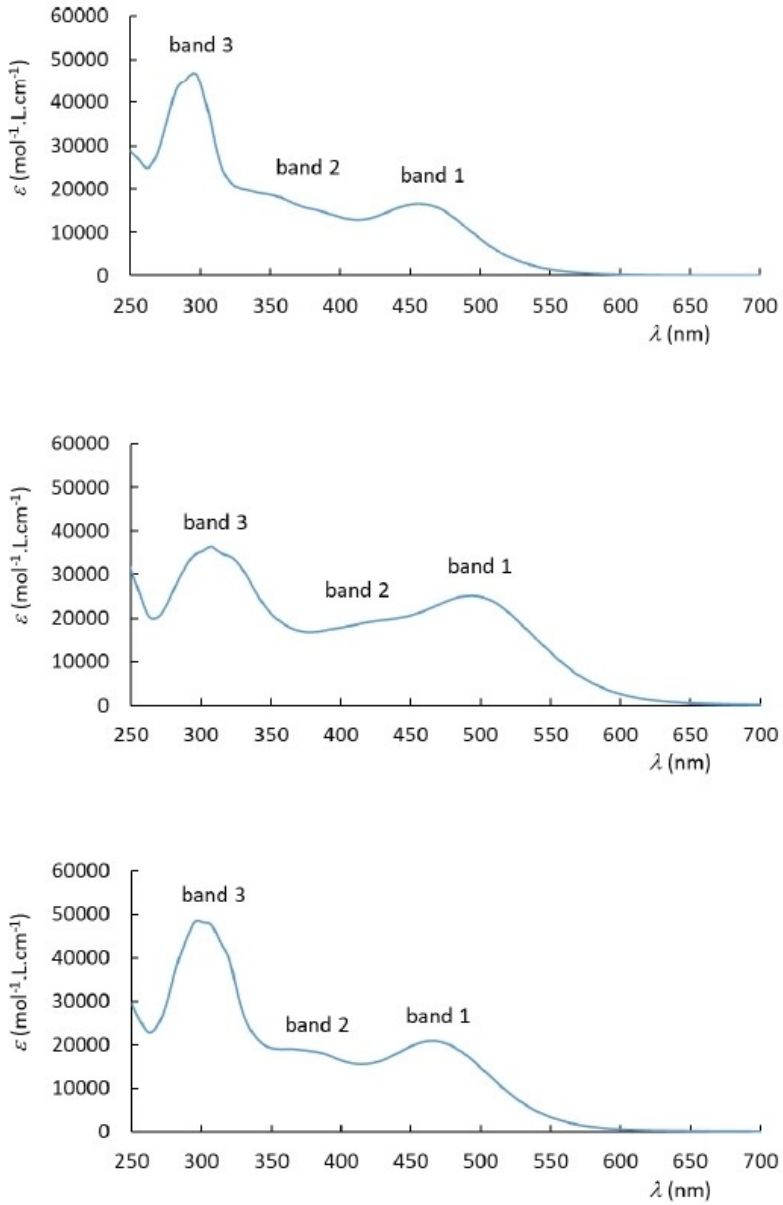

Figure 2. Experimental UV-vis spectra in MeCN for [**1**](PF$_6$)$_3$ (top), [**2**](PF$_6$)$_3$ (middle), and [**3**](PF$_6$)$_3$ (bottom).

The examination of Table 2 indicates that the dominant "push-pull" charge transfer effect is observed in band 1 in any case. Furthermore, the HOMO-LUMO levels provide most of the contribution to the effect. These orbitals are shown in Figure 4. While the LUMO levels are nearly identical with most of the electron density located on the Ru(NO) fragments, the HOMO levels involve the fluorenyl moieties with a contribution of the π-conjugated bridge in $\mathbf{2}^{3+}$ and $\mathbf{3}^{3+}$. This conjugation extension results in a slight enhancement of the energy of the HOMO level and finally in the red shift observed in the UV-visible spectra. The similarities encountered in the spectroscopic properties suggest complexes with rather similar NO$^\bullet$ release capabilities.

NO$^\bullet$ release from [2](PF$_6$)$_3$ and [3](PF$_6$)$_3$

The growing interest devoted to Ru(NO) complexes is largely due to their ability to release nitric oxide under irradiation, according to the following equation (1):

$$(\mathrm{L})\mathrm{Ru^{II}}\text{-}(\mathrm{NO^+}) + \mathrm{solvent} \xrightarrow{h\nu} (\mathrm{L})\mathrm{Ru^{III}}\text{-}\mathrm{solvent} + \mathrm{NO}\cdot \quad (1)$$

Indeed, we have always observed the release of NO as a neutral NO$^\bullet$, thus leading to a subsequent $Ru^{II} \rightarrow Ru^{III}$ conversion during the release process.[11,13,22,26–28] In the class of complexes built up from substituted terpyridine and bipyridine ligand, we have reported on various examples of such behavior with

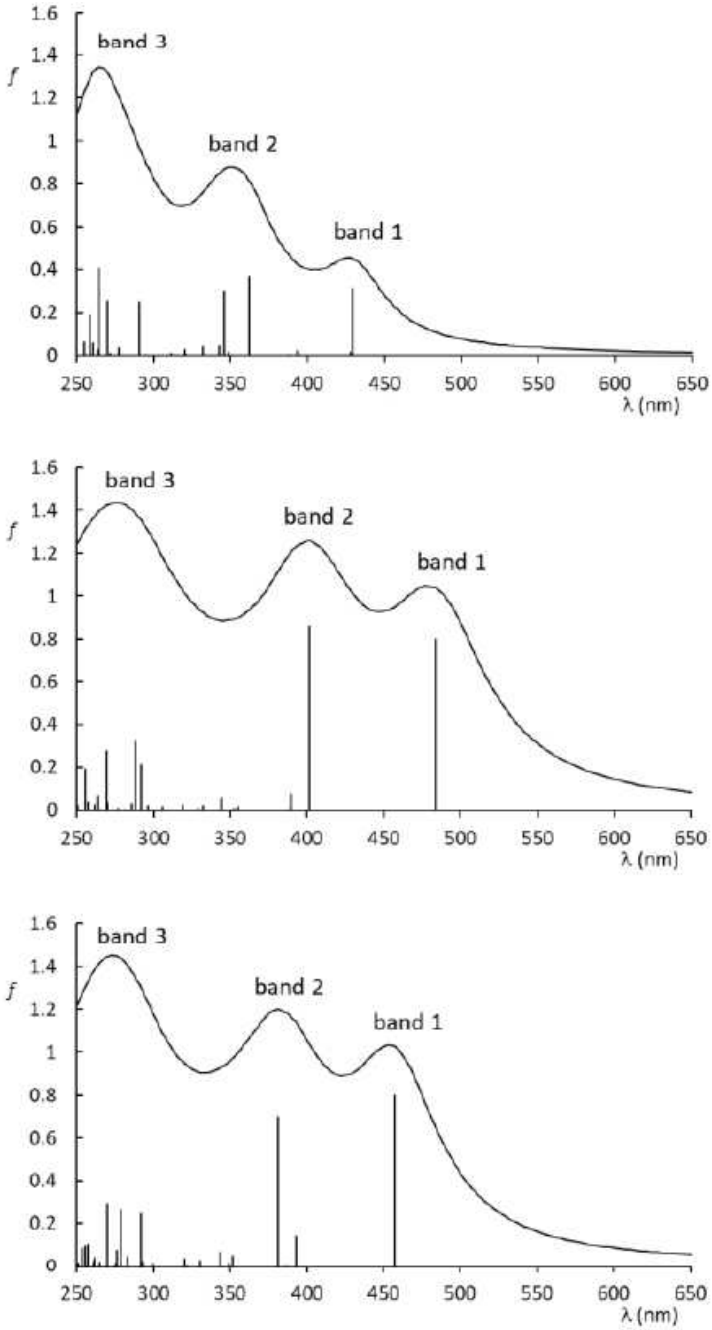

Figure 3. Computed TD-DFT spectra for $\mathbf{1}^{3+}$ (top), $\mathbf{2}^{3+}$ (middle), and $\mathbf{3}^{3+}$ (bottom).

quantum yield (ϕ_{NO}) ranging from 0.004 to 0.03 depending on the donor substituent and the wavelength of irradiation.[11,13,26–28]

The resulting release of nitric oxide is followed by the formation of a solvent bound ruthenium(III) photoproduct, according to equation (1). This was clearly evidenced by X-ray crystallography in the case of a good stability of the Ru^{III} photo product in previous reports.[26,29] Nevertheless, it should be pointed out that equation (1) does not preclude any further chemical evolution of [(L)Ru^{III}(solvent)], with the outcome of a possible photoproduct different than the expected species. Owing to the presence of the lowest energy band (band 1) in the UV-vis spectrum having absorption maxima located at 494 nm and 466 nm for [**2**](PF$_6$)$_3$ and [**3**](PF$_6$)$_3$, respectively, the irradiations were performed at 436 nm using a set of available filters, in order to determine the $NO^{\bullet}$ release efficiencies.

The changes in the electronic absorption spectrum of [**2**](PF$_6$)$_3$ and [**3**](PF$_6$)$_3$ exposed to 436 nm light in acetonitrile are shown in Figure 5. The presence of isosbestic points at 256, 328, 354, 394 nm and 298, 310, 384, 460, 492 nm for [**2**](PF$_6$)$_3$ and [**3**](PF$_6$)$_3$ respectively indicates a clean conversion of the $Ru^{II}(NO^{+})$ complexes to related photolysed species. No back-

Table 2. Details of the dominant transitions involved in band 1 and 2 for $\mathbf{1}^{3+}$, $\mathbf{2}^{3+}$, and $\mathbf{3}^{3+}$: absorption maxima (λ_{max} in nm), oscillator strengths (f), composition of the interaction configuration expansion, and charge transfer character.

Compounds	Transitions	λ_{max}	f	Main composition[a]	Character
$\mathbf{1}^{3+}$	Band 1				
	1→2	430	0.314	78.4% $\chi_{167\rightarrow168}$	fluorene→RuNO
	Band 2				
	1→7	362	0.370	31.3% $\chi_{164\rightarrow169}$ + 18.8% $\chi_{162\rightarrow170}$ + 14.2% $\chi_{159\rightarrow169}$	terpy→RuNO
	1→9	346	0.301	46.1% $\chi_{167\rightarrow170}$ + 20.8% $\chi_{164\rightarrow169}$	fluorene→terpyRuNO
$\mathbf{2}^{3+}$	Band 1				
	1→2	484	0.802	77.3% $\chi_{174\rightarrow175}$	fluorene→RuNO
	Band 2				
	1→5	401	0.855	60.3% $\chi_{174\rightarrow177}$	fluorene→terpy
$\mathbf{3}^{3+}$	Band 1				
	1→2	457	0.802	63.6% $\chi_{173\rightarrow174}$	
	Band 2				
	1→5	393	0.144	67.3% $\chi_{165\rightarrow175}$	bipyRu→RuNO
	1→7	381	0.699	55.2% $\chi_{173\rightarrow176}$ + 10.1% $\chi_{165\rightarrow175}$	fluorene→terpyRuNO

[a] Orbital 167(168) is the HOMO(LUMO) for $\mathbf{1}^{3+}$, 174(175) is the HOMO(LUMO) for $\mathbf{2}^{2+}$, and 173(174) is the HOMO(LUMO) for $\mathbf{3}^{3+}$.

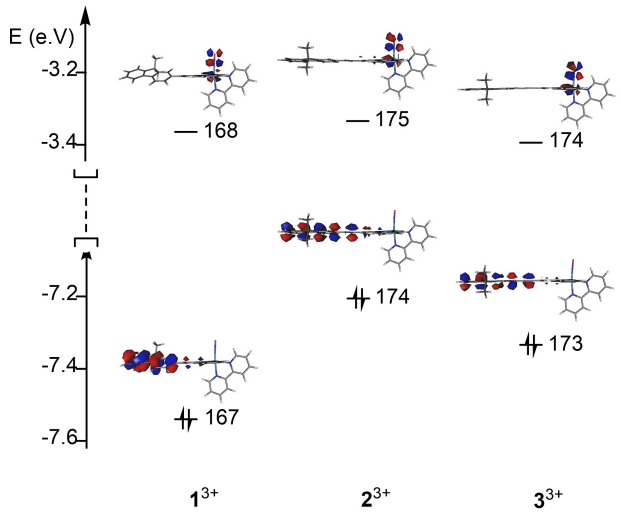

Figure 4. HOMO-LUMO frontier orbitals in $\mathbf{1}^{3+}$, $\mathbf{2}^{3+}$, $\mathbf{3}^{3+}$ with their relative energies.

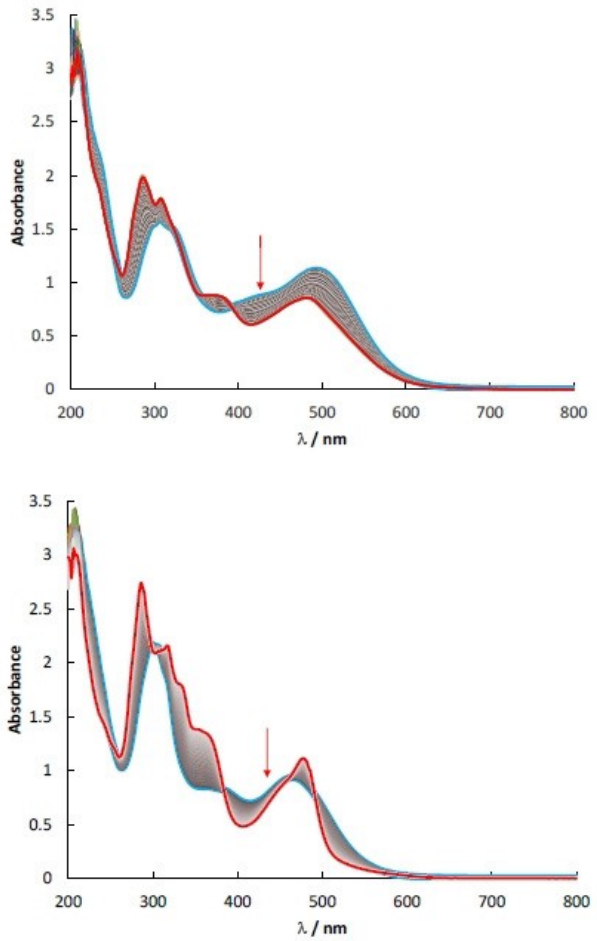

Figure 5. Evolution in the absorption spectra of $[\mathbf{2}](PF_6)_3$ (top) and $[\mathbf{3}](PF_6)_3$ (bottom) in acetonitrile under irradiation at $\lambda = 436$ nm. Blue line: before irradiation; red line: after completeness of the photo-chemical process.

reaction is observed when the light is turned off. In the photolysed species, new bands located at 288, 382, 484 nm and 288, 362, 480 nm arise for $[\mathbf{2}](PF_6)_3$ and $[\mathbf{3}](PF_6)_3$ respectively. Due to a significant absorption of the photoproduct at 436 nm, the release takes 6 hours for $[\mathbf{2}](PF_6)_3$ and 4 hours for $[\mathbf{3}](PF_6)_3$ to reach completeness.

The quantum yield of NO• release (ϕ_{NO}) observed for $[\mathbf{2}](PF_6)_3$ and $[\mathbf{3}](PF_6)_3$ is equal to 0.008 and 0.009 under light irradiation at 436 nm respectively.

Moreover, the photo-generation of NO• can be demonstrated experimentally, by EPR spectroscopy under standard excitation, since spin trapping combined with EPR spectroscopy is considered as one of the best methods for the direct detection of NO• radicals.[30] Namely, we used Iron(II)-N-methyl-D-glucamine dithiocarbamate $[Fe^{II}(MGD)_2]$ to trap NO• due to its high probability of adduct formation and to the high stability of its spin adduct. The appearance of the characteristic triplet signal of NO• is shown in Figure 6, with a hyperfine splitting constant value of $a_N = 1.21 \times 10^{-3}$ cm^{-1} and a g-factor equal to 2.040. These values are fully consistent with the literature report for $[Fe^{II}(MGD)_2\text{-NO}]$ adduct.[31] The weak signal observed in the control spectrum is due to a trace of NO• and related to the fact that the manipulation is never strictly conducted in the dark.

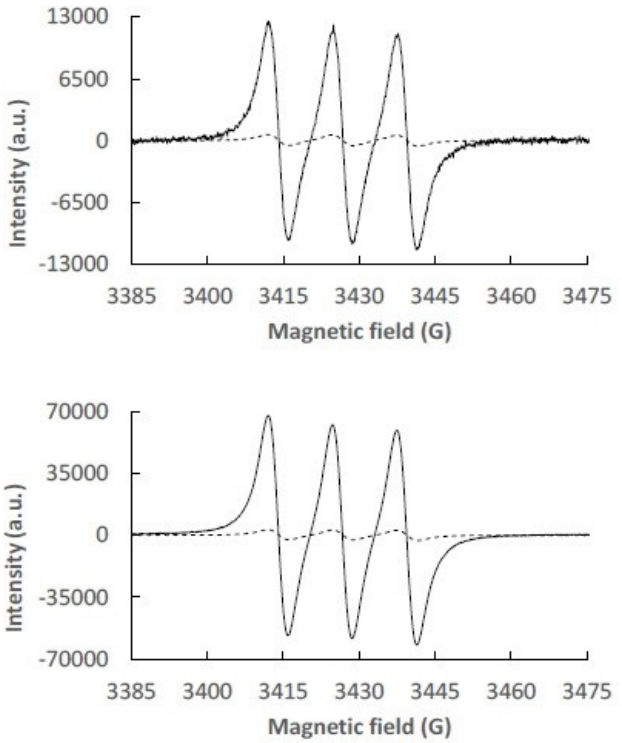

Figure 6. Triplet EPR signals from $NO^{\bullet}$ trapped by $[Fe(MGD)_2]$ for [**2**]$(PF_6)_3$ (top) and [**3**]$(PF_6)_3$ (bottom) upon one photon excitation at room temperature and at $\lambda > 400$ nm (Hg lamp) (bottom). Dashed lines correspond to control signal before irradiation.

The observation of $NO^{\bullet}$ confirms the validity of the process depicted in equation (1) with the outcome of a fast reduction of the concomitant [Ru^{III}(solvent)] species into [Ru^{II}(solvent)], in such a way that no transient Ru^{III} complex is detectable in the reaction medium in the UV-vis spectra (Figure 5). Indeed, the presence of Ru^{III} species leads to the appearance of a broad and weak band at 600 nm.[26] The reasons for a fast reduction of the Ru^{III} species was discussed elsewhere[22] and were related to the presence of 5 pyridine rings in the coordination sphere of the ruthenium center, thus leading to a significant increase of the Ru^{III}/Ru^{II} redox potential, the Ru^{II} being strongly stabilized by d-π^* back donation to the aromatic rings.

Under irradiation at 436 nm, the quantum yield of $NO^{\bullet}$ release is found equal to 0.008, and 0.009 for [**2**]$(PF_6)_3$, and [**3**]$(PF_6)_3$, respectively. These values lie in the same range than the value of 0.011 obtained for [**1**]$(PF_6)_3$, recorded as a reference in the same conditions (*Supplementary Materials*). As a final remark, it is worth pointing out that the NO release process is assumed to arise after photon absorption (equation 1), therefore is regarded as a property related to the evolution of the excited state, without reference to the process (one-photon or two-photon absorption) employed for getting this excited state. In other word, we assume that NO release induced by one or two-photon absorption lead to the same quantum yield. Nevertheless, we have previously observed that fluorenyl-terpyridine based Ru(NO) chromophores can release NO after both one and two-photon excitations.[32]

TPA properties

At the molecular level, the quantification of the simultaneous absorption of two-photons is expressed by the TPA cross-section (σ_{TPA}), expressed in Göppert-Mayer unit (1 GM = 10^{-50} cm^4 s photons^{-1} molecules^{-1}). Due to an absence of fluorescence in the present ruthenium-nitrosyl complexes, the TPA measurements were performed by the Z-scan technique, which requires a good solubility of the investigated molecules at relatively high concentrations (around 10^{-2} mol.L^{-1}) to obtain a good signal to noise ratio. This requirement explains the design of ligands containing two hexyl chains introduced to enhance the solubility of the final complexes. We have previously reported the TPA properties of [**1**]$(PF_6)_3$,[13] therefore the present report focusses on the TPA properties of [**2**]$(PF_6)_3$, and [**3**]$(PF_6)_3$, which are then discussed with reference to those of [**1**]$(PF_6)_3$.

The experimental data were recorded using an incident laser beam at 800 nm. Although it does not correspond strictly to the expected maximum of TPA of the ruthenium complexes (988 nm and 932 nm corresponding to $2\lambda_{max}$ for [**2**]$(PF_6)_3$ and [**3**]$(PF_6)_3$, respectively), it is important to keep in mind that the 800 nm wavelength is a standard laser line produced by femtosecond laser oscillators or laser amplifiers as in the case of our experimental set-up; in addition, it is nearly in the middle range of the therapeutic window (700–950 nm). Therefore, and for practical reasons, it was the one selected here. Figure 7 presents typical normalized transmission (T(z)) (see *Experimental Section*), with the fitting carried out using the standard formalism in Z-scan analysis.[33] The nonlinear absorption was also measured at different energies in the range 40—100 nJ per pulse. As it is expected, the transmission T(z = 0) in each sample decreased as the energy of pulses was increased. It is observed that the Z-scan traces exhibit good symmetry around the z = 0 position. Also, in all cases a good fitting corresponding to TPA was preserved independently of the energy and no artifacts on the Z-scan traces were detected, i.e., thermo-optical effects which usually introduce strong distortion and asymmetries on the signal at high energies. Notice that asymmetric traces can be also a sign of significant generation of photolysed species (irreversible photo-reactions) during the acquisition of Z-scan data. Thus, although photolysed species (after NO release from the excited states generated by TPA) were present in our experiments, their density was not significant and did not affect the measurement of σ_{TPA} for the ruthenium complexes. Other effects such as multistep two-photon excitation (absorption of excited states) that sometimes appears as an artifact of instantaneous TPA was precluded with the use of very short pulses (80 fs). The average of TPA parameters extracted from the Z-scan analyses (nonlinear absorption coefficient β, and molecular TPA cross section σ_{TPA}) are gathered in Table 3 for the two materials. These average values result from several plots of Z-scans for each sample.

Owing to the present data, the issue of the relative effect of double and triple bonds on the TPA properties is naturally addressed in these ruthenium complexes. It is usually assumed that ethynylene-linked (–C≡C–) systems are less conjugated

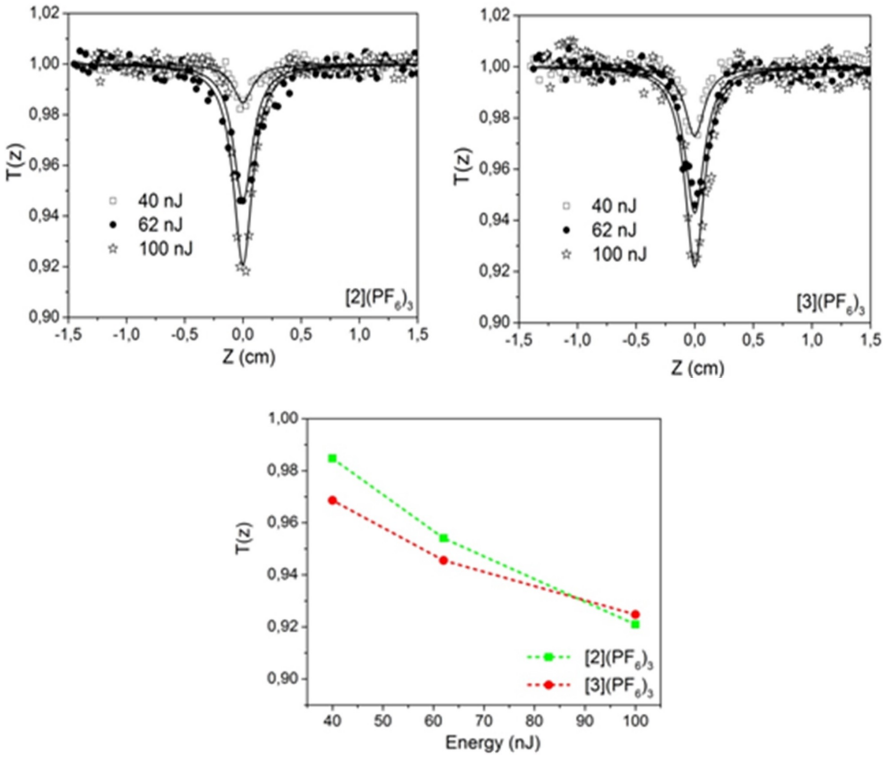

Figure 7. Transmission in Z-scan experiments for [**2**](PF$_6$)$_3$ and [**3**](PF$_6$)$_3$ (top) and decrease in transmission with the increase of pulse energy (bottom). Symbols: experimental data points. Lines: fitting to experimental data.

Table 3. Nonlinear absorption coefficients (β in 10^{-11} cm/W), and TPA cross-sections (σ_{TPA} in GM), for [**1**](PF$_6$)$_3$, [**2**](PF$_6$)$_3$, and [**3**](PF$_6$)$_3$, at the incident laser wavelength of 800 nm.

Compound	β	σ_{TPA}	Ref.
[**1**](PF$_6$)$_3$	2.63 ± 0.43	108 ± 18	[ref 13]
[**2**](PF$_6$)$_3$	3.17 ± 0.45	131 ± 19	this work
[**3**](PF$_6$)$_3$	3.63 ± 0.71	150 ± 29	this work

than vinylene-linked (–CH=CH–) systems, because of energy mismatches between π–π and π^*–π^* levels within the C(sp)–C(sp^2) connection along the π-delocalized skeletons. This leads to larger nonlinear optical responses observed in vinylene systems in most cases.[34]

However, this difference is not pronounced for TPA properties. Indeed, a literature survey indicates reports of larger cross-sections either in the –CH=CH–,[35] or in the –C≡C–[36] classes of chromophores.

Providing a simple picture for the origin and magnitude of the TPA response of the three **1**–**3** ruthenium complexes can be tentatively approached within the framework of a simplified two-level model. At the most fundamental level, σ_{TPA} is related to the imaginary part of the second hyperpolarizability ($Im\gamma$) as follows equation (2):[37]

$$\sigma_{TPA} = \frac{8\pi^2\hbar\omega^2}{n^2c^2} L^4 Im\gamma \quad (2)$$

where ω is the laser frequency, n the refractive index, c the velocity of light in vacuum, and L the local field factor. Within the framework of the perturbation theory, γ can be expressed by an extensive sum-over-state expression, which involves contribution of all $\langle m|\mu|n\rangle = \mu_{mn}$ transitions between states m and n, through the following equation (3):[38]

$$\gamma_{ijkl} = \frac{1}{6\hbar^3} \times P(i,j,k,l) \times \left[\sum_{m\neq 0}\sum_{n\neq 0}\sum_{p\neq 0} \frac{\langle 0|\mu_i|m\rangle\langle m|\mu_j|n\rangle\langle n|\mu_k|p\rangle\langle p|\mu_l|0\rangle}{(\omega_{m0}-\omega-i\Gamma_{m0})(\omega_{n0}-2\omega-i\Gamma_{n0})(\omega_{p0}-\omega-i\Gamma_{p0})} - \sum_{m\neq 0}\sum_{n\neq 0} \frac{\langle 0|\mu_i|m\rangle\langle m|\mu_j|0\rangle\langle 0|\mu_k|n\rangle\langle n|\mu_l|0\rangle}{(\omega_{m0}-\omega-i\Gamma_{m0})(\omega_{n0}-\omega-i\Gamma_{n0})(\omega_{n0}+\omega-i\Gamma_{n0})} \right] \quad (3)$$

In this expression, P is a perturbation operator, 0, m, n, p are the labels of the ground and excited states, i, j, k, l are molecular axis, $\hbar\omega_{m0}$ is the energy of state m, and Γ_{m0} is the band width of the $0 \rightarrow m$ transition.

In the case of pseudo 1-dimensional "push-pull" systems in which the electronic spectra exhibit an intense transition between the ground state (g) to a low-lying excited state (e) with strong charge-transfer character, it was proposed to simplify drastically equation (3) to the dominant contribution of this current charge transfer (g→e) transition. Within this so-called "two-level model", σ_{TPA} is expressed as follows equation (4):[24]

$$\sigma_{TPA} \approx \frac{16\pi^2 f\left(\mu_{ee}-\mu_{gg}\right)^2}{5\hbar^2c^2\Gamma E_{ge}} \quad (4)$$

in which E_{ge} is the energy of the g→e transition, f its oscillator strength, μ_{gg} and μ_{ee} the dipole moment in the ground and excited states, respectively, and Γ the linewidth broadening parameter which is often taken at the constant value of 0.1 eV. Equation 4 is valid at the maximum absorption, when the laser energy ($\hbar\omega$) is half of the transition energy. Nevertheless, we have tentatively applied this model on the basis of the electronic parameters available in the Gaussian09 computation,[39] which indicate that the first (1→2) transition is the only one having high intensity (*f*) low energy (*E*), strong charge transfer (μ_{ee}–μ_{gg}) character for providing an intense TPA response. Experimentally the corresponding UV-visible band 1 accounting for this transition is observed in the $\lambda = 425$–525 nm range, therefore not strictly at half wavelength of the 800 nm output of the Ti-sapphire laser. On the other hand, and apart from the fact that two-photon electronic spectra may be significantly different than one-photon spectra, the 800 nm wavelength was selected for practical reasons as Z-scan experiments with short optical pulses require the use of Ti-sapphire lasers whose emission is precisely around 800 nm. Further, this wavelength is within the window of biomedical interest for medical therapy based on light. Of course, extending the laser emission to other wavelength would be possible but it cannot be envisioned practically, for a question of high cost when laser sources of short pulses are used. Under these assumptions, the computed two-level evolution of σ_{TPA} on going from $\mathbf{1}^{3+}$ to $\mathbf{2}^{3+}$ and $\mathbf{3}^{3+}$ are estimated in Table 4 and compared with the experimental data.

The observation that the two-level approach fails to account for the effect of double and triple bond insertion in [**2**](PF$_6$)$_3$, and [**3**](PF$_6$)$_3$ immediately strikes in Table 4. Indeed, the experimental σ_{TPA} enhancement appears far reduced compared to the computed prediction. The issue of a possible saturation observed experimentally in TPA material of long length has been discussed in the literature.[15] As the π-system becomes longer, it reaches a length known as the "conjugation length", beyond which the loss of planarity leads to electron density confinement along the conjugated chains. However, this possibility cannot be envisioned here, because $\mathbf{2}^{3+}$ and $\mathbf{3}^{3+}$ appear more planar than the reference $\mathbf{1}^{3+}$. Additionally, there is no simple expression to relate the dependence of the parameters of equation 4 (*f*, μ_{ee}-μ_{gg}, E_{ge}) and hence that of σ_{TPA}, on the size of a molecule. A more fruitful approach is to use the concept of normalized cross-section (σ_{TPA}/Ne) which refers to the cross-section per π-electron.

Several investigations have been reported in the literature with the aim of finding the optimized size to maximize σ_{TPA}/Ne.[40–42] Saturation effects can take place in the case of systems of much bigger size than the present $\mathbf{2}^{3+}$ and $\mathbf{3}^{3+}$ species. Therefore, one can conclude that the modest enhancement observed in the σ_{TPA} value after introduction of double and triple C–C bond is not due to the loss of conjugation frequently encountered in large size chromophores. Instead, one may infer that the two-level expression of σ_{TPA} (equation 4) cannot fully account for providing a simple expression of the origin of the TPA properties along this series, in part due to some energy mismatches between the real absorption maxima and the experimental requirement to have to work at incident wavelength of the Ti-sapphire laser (800 nm).

After the observation of a modest σ_{TPA} enhancement obtained within the present "push-pull" approach, the issue of a more promising strategy is naturally addressed. It has recently been reported that huge σ_{TPA} enhancement could be accessible in complexes of higher dimensionality than those of the first generation of "push-pull" chromophores.[43] Investigating multipolar chromophores will certainly require more sophisticated synthetic approaches and computational analysis, to optimize the best candidates. Nevertheless, we are now focusing our research efforts in these directions.

Conclusion

With the aim of increasing the TPA properties of a Ru(NO) complex capable of releasing NO$^\bullet$ under irradiation in the therapeutic window, a strategy based on inserting double and triple carbon-carbon bond was explored within a family of "push-pull" species in which the nitrosyl ligand acts as the electron acceptor and the fluorenyl moieties act as the electron donor. This leads to two new Ru(NO) complexes perfectly characterized and capable of releasing NO with a quantum yield of 0.01. The extension of the π-delocalized framework, leads to an enhancement of the TPA cross-section from 108 to 150 GM, which is lower than the value predicted using the crude but commonly used "two-level" prediction. Although there is no clear evidence for a TPA saturation in these species, the present investigation suggests that the most efficient NO$^\bullet$ donors in the family of Ru(NO) complexes would certainly benefit from geometries of greater complexity than that of the first generation of 1-dimensional ("push-pull") systems. In this regard, an enhancement of conjugation between structural fragments of such complexes would result in enhanced TPA response and consequently of their NO$^\bullet$ release capabilities via the uncaging cross section ($\sigma_{TPA} \times \phi_{NO}$).

Table 4. Experimental cross-sections (σ_{TPA} in GM) compared with the computed data: Energies (E_{ge} in eV), oscillator strength (*f*), change in dipole moment during transition (μ_{ee}–μ_{gg} in D).

	Experimental data		Computed data (equation 4)			
compound	σ_{TPA}	Relative[a] σ_{TPA}	E_{ge}	*f*	μ_{ee}–μ_{gg}	relative[1] σ_{TPA}
[**1**](PF$_6$)$_3$	108	**1**	2.886	0.314	31.39	**1**
[**2**](PF$_6$)$_3$	131	**1.21**	2.563	0.802	36.12	**3.81**
[**3**](PF$_6$)$_3$	150	**1.39**	2.712	0.802	37.05	**3.79**

[a] [**1**](PF$_6$)$_3$ being used as the reference.

Experimental Section

Materials and Equipment

Methylacrylate, triethylamine, diisobutylaluminum hydride (DIBAL–H) solution in toluene, $Pd(PPh_3)_2Cl_2$, $Pd(CH_3COO)_2$, CuI were purchased from Sigma-Aldrich; LiCl, NH_4PF_6, 2-acetylpyridine and 2-bromofluorene from Alfa Aesar; 2,2′-bipyridine, ethyl pyridine-2-carboxylate, ethynyltrimethylsilane, trifluoromethanesulfonic anhydride, $Pd(PPh_3)_4$, Pd(*o*-tol)$_3$ from TCI; $NaNO_2$ from Fluka, $RuCl_3 \cdot xH_2O$ (Ru: 40–49%) from STREM. Chemicals and solvents were analytical grade and used without further purification. [**1**]$(PF_6)_3$[13] and **3c**, **3d**, **3e**[21] were prepared as previously described.

Elemental analyses were performed at LCC with a Perkin–Elmer 2400 series II Instrument. The ^{1}H NMR and ^{13}C NMR spectra were recorded at 298 K with a Bruker Avance 400 spectrometer, using $CDCl_3$, CD_3OD or CD_3CN as an internal reference. The IR spectra were recorded with a Perkin–Elmer (FTIR/FIR) 100 Spectrometer. The ESI mass spectra were performed on a UPLC Xevo G2 Q TOF (Waters) spectrometer and Bruker Daltonics–micrOTOF–Q III spectrometer. UV-Vis spectra were obtained on a Perkin Elmer Lambda 35 UV-Vis spectrometer. Electron paramagnetic resonance experiments (EPR) were performed on a Bruker ESP 500E spectrometer. The atom labeling for the complete assignment of [**2**]$(PF_6)_3$, and [**3**]$(PF_6)_3$ by NMR spectroscopy is provided in Supplementary Materials.

Synthesis

Synthesis of ***2a****.* 2-Bromofluorene (11.65 g, 0.048 mol) and KI (0.79 g, 4.76 mmol) were dissolved in DMSO (96 mL) upon slight heating. After complete dissolution the mixture was degassed and placed under inert atmosphere. KOH (9.16 g, 0.164 mol) was then pestled and added carefully to the solution under Ar flow. The mixture was stirred for 20 min followed by slow, dropwise addition of *n*-bromohexane (17 mL, 0.121 mol) in 5 portions under vigorous stirring. The interval between portions was 10 min. After the addition was completed, the mixture was left stirring at room temperature for 3 hours followed by water addition and extraction with EtOAc. The organic layer was washed with brine and dried over Na_2SO_4, and the solvent was evaporated under reduced pressure. The product was purified by column chromatography (eluent: pentane, 100%) with a quantitative yield of 19.63 g of **2a** as a colorless oil. ^{1}H NMR (300 MHz, $CDCl_3$) δ 7.70–7.64 (m, 1H), 7.56 (d, *J* = 7.5, 1H), 7.46 (s, 1H), 7.45 (dd, *J* = 8.0, 1.9 Hz, 1H), 7.34–7.31 (m, 3H), 2.02–1.85 (m, 4H), 1.19–0.97 (m,12H), 0.78 (t, *J* = 7.0 Hz, 6H), 0.69–0.51 (m, 4H).

Synthesis of ***2b****.* Methylacrylate (1.35 mL, 15 mmol) and anhydrous DMF (10 mL) were added to the mixture of **2a** (4.13 g, 10 mmol), $Pd(OAc)_2$ (67 mg, 0.30 mmol), P(*o*-tol)$_3$ (228 mg, 0.75 mmol) and Et_3N (1.4 mL, 10 mmol) under inert atmosphere. The resulting suspension was heated at 90 °C under vigorous stirring over 14 h. After the completion of the reaction, the suspension was cooled down to room temperature followed by adding water (100 mL). The mixture was extracted with EtOAc; the organic extracts were washed with brine, dried over Na_2SO_4 and filtrated. The solvent was evaporated under reduced pressure and the residues were purified by column chromatography (eluent: *n*-hexane/acetone, 100:2) on silica gel to yield 3.43 g (8.20 mmol, 82%) of **2b** as a yellow oil. ^{1}H NMR (400 MHz, $CDCl_3$) δ 7.79 (d, *J* = 16.0 Hz, 1H), 7.74–7.66 (m, 2H), 7.51 (dd, *J* = 7.9, 1.6 Hz, 1H), 7.49 (d, *J* = 1.6 Hz, 1H), 7.36–7.32 (m, 3H), 6.50 (d, *J* = 16.0 Hz, 1H), 3.83 (s, 3H), 2.01–1.93 (m, 4H), 1.14–1.00 (m, 12H), 0.76 (t, *J* = 7.1 Hz, 6H), 0.65–0.56 (m, 4H); ^{13}C NMR (100 MHz, $CDCl_3$), δ 167.80, 151.50, 151.48, 145.68, 143.79, 140.31, 133.27, 127.96, 127.58, 127.07, 123.10, 122.47, 120.30, 120.15, 116.80, 55.23, 51.81, 40.46, 31.60, 29.79, 23.86, 22.69, 14.12. HRMS (ESI): calculated for $C_{29}H_{39}O_2$ $(M+H)^+$: 419.2944, found: 419.2946.

Synthesis of ***2c*** *and* ***2d****.* The solution of DIBAL–H (30 mL, 1.5 M, 45 mmol) was added dropwise into the solution of **2b** (6.28 g, 15 mmol) in anhydrous toluene (150 mL) under inert atmosphere at −78 °C. The reaction mixture was stirred vigorously until the complete disappearance of the starting material (TLC control). Then MeOH (3.6 mL) was added slowly to the reaction mixture until complete evolution of H_2 followed by quick addition of AcOEt (300 mL). The mixture was allowed to reach room temperature and stirring vigorously for 1 hour followed by filtration through celite; the filtrate was evaporated under reduced pressure. The resulting mixture was dissolved in $CHCl_3$ (225 mL) and MnO_2 (9.78 g, 112.5 mmol) was added. The heterogeneous mixture was stirred at room temperature until complete disappearance of starting material (TLC control, for 2–3 days). After completion of the reaction, the mixture was filtered through celite and the filtrate was concentrated under reduced pressure. The residues were purified by column chromatography (eluent: *n*-hexane/EtOAc, 99:1) on silica gel to yield 3.43 g (8.2 mmol, 70%) of **2d** as a yellow oil. ^{1}H NMR of compound 2d (300 MHz, $CDCl_3$), δ 9.74 (d, *J* = 7.7 Hz, 1H), 7.77–7.70 (m, 2H), 7.58 (d, *J* = 15.9 Hz, 1H), 7.56 (dd, *J* = 7.9, 1.6 Hz, 1H), 7.53 (d, *J* = 1.6 Hz, 1H), 7.39–7.34 (m, 3H), 6.79 (dd, *J* = 15.9, 7.7 Hz, 1H), 2.03–1.94 (m, 4H), 1.15–0.97 (m, 12H), 0.75 (t, *J* = 6.9 Hz, 6H), 0.67–0.55 (m, 4H); NMR ^{13}C (75 MHz, $CDCl_3$) δ 193.88, 153.74, 151.72, 151.62, 144.83, 140.04, 132.88, 128.34, 128.18, 127.84, 127.17, 123.15, 122.82, 120.51, 120.34, 55.30, 40.42, 31.59, 29.76, 23.85, 22.68, 14.11. HRMS (ESI): calculated for $C_{28}H_{37}O$ $(M+H)^+$: 389.2839, found: 389.2840.

Synthesis of ***2e****.* A solution of NaOH (1.35 mL, 1 M, 1.35 mmol) in water was added into the solution of **2d** (0.35 g, 0.90 mmol) and 2-acetylpyridine (0.10 mL, 0.90 mmol) in EtOH under vigorous stirring. The reaction mixture was stirred at room temperature until complete conversion of starting material (TLC control). The resulting precipitate was filtered off, rinsed with water and cold EtOH and dried under vacuum to give **2e** (0.20 g, 0.52 mmol) in 45% yield. After purification of the filtrate by column chromatography (elution system: hexane–AcOEt, 9:1) additional 0.06 g were obtained (13%). The total yield was 58%, yellow powder; mp. 104–105 °C; ^{1}H NMR (400 MHz, THF-d_8) δ 8.69 (ddd, *J* = 4.7, 1.7, 0.9 Hz, 1H), 8.11 (ddd, *J* = 7.7, 1.3, 0.9 Hz, 1H), 7.93 (d, *J* = 15.4 Hz, 1H), 7.90 (ddd, *J* = 7.7, 7.5, 1.7 Hz, 1H), 7.77–7.65 (m, 3H), 7.65 (d, *J* = 1.5 Hz, 1H), 7.55 (dd, *J* = 7.9, 1.5 Hz, 1H), 7.50 (ddd, *J* = 7.5, 4.7, 1.3 Hz, 1H), 7.41–7.33 (m, 1H), 7.35–7.23 (m, 3H), 7.19 (d, *J* = 15.4 Hz, 1H), 2.14–1.97 (m, 4H), 1.17–0.96 (m, 12H), 0.75 (t, *J* = 7.0 Hz, 6H), 0.70–0.55 (m, 4H); ^{13}C NMR (100 MHz, THF-d_8) δ 189.02, 155.49, 152.11, 151.99, 149.76, 144.95, 143.52, 143.21, 141.70, 137.78, 136.70, 128.34, 128.06, 127.80, 127.78, 127.54, 125.09, 123.68, 123.07, 122.29, 120.85, 120.84, 55.93, 41.28, 32.49, 30.69, 24.70, 23.48, 14.37. HRMS (ESI): calculated for $C_{35}H_{42}NO$ $(M+H)^+$: 492.3261, found: 491.3261.

Synthesis of ligand ***A****.* 1-(2-Oxo-2-(pyridin-2-yl)ethyl)pyridin-1-ium iodide (0.32 g, 0.99 mmol) and ammonium acetate (1.04 g, 13.5 mmol) were added to the suspension of **2e** (0.44 g, 0.9 mmol) in EtOH (5 mL) and the mixture was refluxed until complete conversion of starting ketone **2e** (TLC control). After the reaction finished the mixture was cooled down and the solvent was evaporated under reduced pressure. The residue was diluted with water and extracted with EtOAc. The organic extracts were dried over Na_2SO_4 followed by filtration and solvent evaporation under reduced pressure. The residue was purified two times by column chromatography on alumina, using CH_2Cl_2 in the first column; hexane /acetone, 9:1 for the second column to yield 0.19 g (0.32 mmol, 36%) of the ligand ***A*** as a yellow oil. ^{1}H NMR (400 MHz, CD_3CN) δ 8.72 (ddd, *J* = 4.8, 1.8, 0.9 Hz, 2H), 8.66 (ddd, *J* = 7.8, 1.2, 0.9 Hz, 2H), 8.64 (s, 2H), 7.95 (ddd, *J* = 7.8, 7.6, 1.8 Hz, 2H), 7.79–7.75

(m, 3H), 7.68 (d, J=16.4 Hz, 1H), 7.65 (dd, J=7.8, 1.5 Hz, 1H), 7.48 (d, J=16.4 Hz, 1H), 7.43 (ddd, J=7.6, 4.8, 1.2 Hz, 2H), 7.43–7.40 (m, 1H), 7.37–7.31 (m, 2H), 2.12–1.98 (m, 4H), 1.14–0.94 (m, 12H), 0.73 (t, J=7.0 Hz, 6H), 0.62–0.45 (m, 4H); NMR ^{13}C (100 MHz, CD_3CN) δ 156.93, 156.78, 152.32, 152.07, 150.23, 148.02, 142.88, 141.59, 138.09, 136.58, 134.57, 128.44, 127.98, 127.7, 126.89, 125.13, 124.00, 122.45, 121.91, 120.88, 120.83, 118.65, 56.02, 40.82, 32.18, 30.21, 24.64, 23.16, 14.20. HRMS (ESI): calculated for $C_{42}H_{46}N_3$ $(M+H)^+$: 592.3686, found: 592.3689.

*Synthesis of **3a** and **3b**.* The mixture of **2a** (3.14 g, 7.60 mmol), activated CuI (72 mg, 0.38 mmol) and $PdCl_2(PPh_3)_2$ (133 mg, 0.189 mmol) was placed under inert atmosphere followed by addition of anhydrous THF (10 mL). The reaction mixture was heated to reflux followed by dropwise addition of DIPA (6 mL, 43 mmol) and ethynyltrimethylsilane (2.7 mL, 19 mmol), the condenser being intensively chilled (the boiling point of ethynyltrimethylsilane is 57 °C). After 12 h, the solution was cooled down, and EtOAc (15 mL) was added followed by washing with saturated NH_4Cl solution. The product was purified by column chromatography (eluent: hexane, 100%) over silica gel to yield 1.84 g (4.26 mmol, 56%) of **3a**, which was then suspended in the mixture of methanol (10 mL) and diethyl ether (10 mL) followed by potassium carbonate addition (2.11 g, 15 mmol). The mixture was stirred for 90 min and filtered, the filtrate was evaporated under reduced pressure. The residue was dissolved in hexane and filtered through silica gel which was thoroughly rinsed with hexane. The filtrate was evaporated under reduced pressure to yield 1.24 g (3.46 mmol, 81%) of **3b** as a colorless oil. ^{1}H NMR of compound **3b** (400 MHz, $CDCl_3$) δ 7.73–7.70 (m, 1H), 7.67 (dd, J=7.0, 1.3 Hz, 1H), 7.51 (dd, J=7.0, 1.4 Hz, 1H), 7.50 (s, 1H), 7.40–7.31 (m, 3H), 3.14 (s, 1H), 2.01–1.95 (m, 4H), 1.22–0.98 (m, 12H), 0.79 (t, J=7.1 Hz, 6H), 0.68–0.56 (m, 4H); ^{13}C NMR (100 MHz, $CDCl_3$) δ 151.2, 150.9, 142.1, 140.4, 131.2, 127.8, 127.0, 126.7, 123.0, 120.3, 120.2, 119.7, 84.9, 77.0, 55.2, 40.5, 31.6, 29.8, 23.8, 22.7, 14.1.

*Synthesis of ligand **B**.* The mixture of **3e** (311 mg, 0.87 mmol), **3b** (330 mg, 0.87 mmol), $[Pd(PPh_3)_4]$ (50 mg, 0.043 mmol) was degassed and placed under inert atmosphere. Anhydrous toluene (60 mL) and DIPA (8.2 mL) were added to the reaction mixture and the resulting mixture was heated at 80 °C over 36 h. After completion of the reaction (progress controlled by TLC), the reaction mixture was cooled down and evaporated under reduced pressure. The residue was dissolved in CH_2Cl_2, rinsed with water, brine and dried over Na_2SO_4. The solvent was evaporated at reduced pressure. The product was purified by two successive column chromatography on silica gel: 1) elution with pentane/CH_2Cl_2, 9:1; 2) elution with pentane/EtOAc, 10:1 to yield 213 mg (42%) of ligand ***B***, as a yellowish oil. ^{1}H NMR (400 MHz, $CDCl_3$) δ 8.74 (dd, J=4.7, 1.7 Hz, 2H), 8.64 (m, 4H), 7.92–7.82 (td, J=7.7, 1.7 Hz, 2H), 7.75–7.68 (m, 2H), 7.58 (s, 1H), 7.57 (d, J=8.5 Hz, 1H), 7.40–7.30 (m, 5H), 2.08–1.92 (m, 4H), 1.20–0.99 (m, 12H), 0.80 (t, J=7.0 Hz, 6H), 0.72–0.55 (m, 4H). ^{13}C NMR (100 MHz, $CDCl_3$) δ 155.8, 155.6, 151.3, 151.0, 149.3, 142.3, 140.3, 137.0, 133.8, 131.0, 127.8, 127.0, 126.6, 124.1, 123.0, 122.9, 121.3, 120.6, 120.3, 119.8, 95.3, 87.7, 55.3, 40.5, 31.6, 29.8, 23.9, 22.7, 14.1. HRMS (APCI): calculated for $C_{42}H_{43}N_3$ $(M)^+$: 589.3451, found: 589.3438.

General procedure for the synthesis of Ru(L)Cl_3: Ligands **A** or **B** (1 mmol) and $RuCl_3 \cdot xH_2O$ (Ru: 40–49%; 251 mg for 1 mmol of ligand, 1–1.22 eq.) were suspended in ethanol (65 mL for 1 mmol of ligand). The mixture was refluxed over 3 h; the flask was covered with aluminum foil to protect the complex from light. After 3 h the flask was cooled down and the volume of solvent was reduced to 1/3 of the initial volume upon evaporation under reduced pressure. The residue was left in the fridge at 5 °C for 2 h. The obtained precipitate was filtered off and was thoroughly rinsed with cold water, chilled EtOH and diethyl ether. The complex was dried under vacuum to yield brown-black solids.

Ru(A)Cl_3: yield 90%. Ru(B)Cl_3: yield 58%.

General procedure for synthesis of [Ru(L)(bipy)Cl]Cl: Complex *Ru(L)Cl_3* (1 equiv), 2,2′-bipyridine (1 equiv), LiCl (6 equiv) were added to the mixture of 75% EtOH/25% H_2O mixture (92 mL for 1 mmol of *Ru(L)Cl_3*), followed by Et_3N (1.6 equiv) addition. The mixture was refluxed for 3 h; the flask was covered with aluminum foil to protect the complex from light. After completion of the reaction, an undesired precipitate was filtered off from the hot solution. The precipitate was washed by ethanol and the filtrate was concentrated under reduced pressure to 1/6 of the initial volume and kept in the fridge at 5 °C over 2 h. The obtained precipitate was filtered off and thoroughly rinsed with aqueous HCl solution (3 M), a small amount of chilled EtOH and diethyl ether. The product was dried under the vacuum to yield purple solids.

[Ru(**A**)(bipy)Cl]Cl: yield 69%. ^{1}H NMR (400 MHz, CD_3OD) δ 10.29 (d, J=5.1 Hz, 1H), 8.89 (s, 2H), 8.78 (d, J=8.0 Hz, 1H), 8.56 (d, J=7.8 Hz, 2H), 8.49 (d, J=8.0 Hz, 1H), 8.31 (t, J=7.8 Hz, 1H), 8.10 (d, J=16.3 Hz, 1H), 8.05–8.00 (m, 1H), 7.88–7.65 (m, 9H), 7.59 (d, J=16.3 Hz, 1H), 7.42 (ddd, J=8.3, 6.7, 3.5 Hz, 4H), 7.33–7.26 (m, 2H), 7.05 (t, J=6.5 Hz, 1H), 2.23–2.07 (m, 4H), 1.17–1.00 (m, 12H), 0.78 (t, J=7.0 Hz, 6H), 0.72–0.59 (m, 4H).

[Ru(**B**)(bipy)Cl]Cl: yield 83%. ^{1}H NMR (400 MHz, CD_3OD) δ 10.23 (d, J=5 Hz, 1H), 8.82 (s, 2H), 8.79 (d, J=8.2 Hz, 1H), 8.57 (d, J=8.0 Hz, 2H), 8.50 (d, J=7.9 Hz, 1H), 8.34 (td, J=7.9, 1.5 Hz, 1H), 8.02 (ddd, J=7.5, 5.6, 1.2 Hz, 1H), 7.91 (td, J=7.9, 1.5 Hz, 2H), 7.87 (d, J=7.8 Hz, 1H), 7.85–7.83 (m, 1H), 7.78–7.67 (m, 5H), 7.47–7.38 (m, 4H), 7.35 (ddd, J=7.6, 5.5, 1.3 Hz, 2H), 7.06 (ddd, J=7.3, 5.8, 1.3 Hz, 1H), 2.14–2.07 (m, 4H), 1.19–0.99 (m, 12H), 0.79 (t, J=7.0 Hz, 6H), 0.66–0.56 (m, 4H).

General procedure for synthesis of [Ru(L)(bipy)NO_2]Cl: Complex *[Ru(L)(bipy)Cl]Cl* (1 equiv) and $NaNO_2$ (10 equiv) were dissolved in 75% EtOH/25% H_2O mixture (124 mL for 1 mmol of *[Ru(L)(bipy)Cl]Cl*). The mixture was refluxed over 3 h; the flask was covered with aluminum foil to protect the complex from light. After completion of the reaction, the flask was cooled down and the volume of solvent was reduced to 1/6 of the initial volume. The residue was kept at 5 °C, for 2 h. The obtained precipitate was filtrated off and rinsed with cold water, a small amount of cold EtOH and diethyl ether. The complex was dried under the vacuum to yield dark red solids.

[Ru(**A**)(bipy)NO_2]Cl: yield 66%. ^{1}H NMR (400 MHz, CD_3OD) δ 9.91 (d, J=4.8 Hz, 1H), 8.78 (d, J=8.1 Hz, 1H), 8.74 (s, 2H), 8.55 (d, J=8.1 Hz, 1H), 8.46 (d, J=8.0 Hz, 2H), 8.32 (td, J=8.0, 1.5 Hz, 1H), 8.04–7.99 (m, 1H), 7.96 (d, J=16.3 Hz, 1H), 7.92–7.80 (m, 6H), 7.77–7.73 (m, 2H), 7.73–7.68 (m, 1H), 7.52 (d, J=16.3 Hz, 1H), 7.47–7.43 (m, 2H), 7.42–7.36 (m, 2H), 7.36–7.31 (m, 2H), 7.19–7.13 (m, 1H), 2.21–2.07 (m, 4H), 1.16–1.00 (m, 12H), 0.76 (t, J=7.0 Hz, 6H), 0.70–0.58 (m, 4H).

[Ru(**B**)(bipy)NO_2]Cl: yield 46%. ^{1}H NMR (400 MHz, CD_3OD) δ 9.90 (d, J=5.3 Hz, 1H), 8.78 (d, J=8.2 Hz, 1H), 8.76 (s, 2H), 8.55 (d, J=8.1 Hz, 1H), 8.50 (d, J=8.0 Hz, 2H), 8.34 (td, J=7.9, 1.4 Hz, 1H), 8.02 (ddd, J=7.5, 5.9, 1.1 Hz, 1H), 7.93 (td, J=7.9, 1.4 Hz, 2H), 7.90–7. 81 (m, 3H), 7.79 (s, 1H), 7.75 (d, J=8.6 Hz, 2H), 7.67 (dd, J=7.8, 1.3 Hz, 1H), 7.52–7.32 (m, 6H), 7.18 (ddd, J=7.6, 5.7,1.3 Hz, 1H), 2.19–2.00 (m, 4H), 1.21–1.01 (m, 12H), 0.78 (t, J=6.9 Hz, 6H), 0.70–0.54 (m, 4H).

General procedure for synthesis of [Ru(L)(bipy)NO]$(PF_6)_3$: Complex [Ru(L)(bipy)NO_2]Cl (1 equiv) was dissolved in EtOH (108 mL for 1 mmol of [Ru(L)(bipy)NO_2]Cl), and the solution was mixed with the solution of HCl (12 M, 108 mL for 1 mmol of [Ru(L)(bipy)NO_2]Cl, 1300 equiv) in EtOH (216 mL for 1 mmol of [Ru(L)(bipy)NO_2]Cl). The mixture was heated to 60 °C and allowed to stand under stirring for

1 h; the flask was covered by aluminum foil to protect the complex from light. After completion of the reaction, the flask was cooled down and the volume of solvent was reduced to 1/5 of the initial volume followed by addition of saturated solution of NH_4PF_6 (15 equiv) in water. The mixture was kept at 5 °C for 2 h. The obtained precipitate was filtrated off, rinsed with a small amount of cold EtOH and diethyl ether. The complex was dried under vacuum.

[**2**](PF$_6$)$_3$: yield 63 %. ^{1}H NMR (400 MHz, CD_3CN) δ 9.30 (d, *J* = 5.7 Hz, 1H), 8.92 (s, 2H), 8.81 (d, *J* = 7.8 Hz, 1H), 8.74 (d, *J* = 7.4 Hz, 2H), 8.69 (td, *J* = 8.1, 1.4 Hz, 1H), 8.61 (d, *J* = 7.7 Hz, 1H), 8.49 (td, *J* = 7.9, 1.4 Hz, 2H), 8.32 (d, *J* = 16.3 Hz, 1H), 8.33–8.27 (m, 1H), 8.27–8.23 (m, 1H), 8.01 (dd, *J* = 5.6, 1.1 Hz, 2H), 7.95 (d, *J* = 8.1 Hz,1H), 7.94 (s, 1H), 7.90–7.83 (m, 2H), 7.74 (d, *J* = 16.2 Hz, 1H), 7.71 (ddd, *J* = 7.5, 5.4, 1.1 Hz, 2H), 7.53–7.39 (m, 4H), 7.32 (dd, *J* = 6.0, 0.9 Hz, 1H), 2.21–2.09 (m, 4H), 1.15–0.97 (m, 12H), 0.77 (t, *J* = 6.9 Hz, 6H), 0.67–0.52 (m, 4H). Elemental analysis calcd (%) for $C_{52}H_{53}N_6ORuP_3F_{18}$: C 47.53, H 4.07, N 6.40; found: C 47.26, H 4.09, N 6.74. IR (neat film): 2929 cm^{-1}, 1942 cm^{-1} ν(NO), 1592 cm^{-1}, 1481 cm^{-1}, 1046 cm^{-1}, 836 cm^{-1} (PF$_6$), 557 cm^{-1}.

[**3**](PF$_6$)$_3$: yield 66 %. ^{1}H NMR (300 MHz, CD_3CN) δ 9.31 (d, *J* = 5.8 Hz, 1H), 8.96 (s, 2H), 8.82 (d, *J* = 8.1 Hz, 1H), 8.75–8.66 (m, 3H), 8.63 (d, *J* = 8.1 Hz, 1H), 8.48 (t, *J* = 8.2 Hz, 2H), 8.31 (t, *J* = 8.0, 1H), 8.28–8.21 (m, 1H), 8.02 (d, *J* = 5.2 Hz, 2H), 7.97 (d, *J* = 7.8 Hz, 1H), 7.92–7.79 (m, 3H), 7.78–7.68 (m, 2H), 7.56–7.39 (m, 4H), 7.34 (d, *J* = 5.9 Hz, 1H), 2.27–2.05 (m, 4H), 1.21–0.95 (m, 12H), 0.77 (t, *J* = 6.8 Hz, 6H), 0.66–0.46 (m, 4H). Elemental analysis calcd (%) for $C_{52}H_{51}N_6ORuP_3F_{18}$: C 47.60, H 3.92, N 6.41; found: C47.61, H 3.66, N 6.42. IR (neat film): 2927 cm^{-1}, 2201 cm^{-1} ν(C≡C), 1945 cm^{-1} ν(NO), 1600 cm^{-1}, 1480 cm^{-1}, 835 cm^{-1} (PF$_6$), 557 cm^{-1}.

Computational studies

The ruthenium complexes [**2**]$^+$, and [**3**]$^{3+}$ were fully optimized in gas phase using the Gaussian-09 program package[44] within the framework of the Density Functional Theory (DFT). The double-ζ basis set 6–31G* was used for all atoms except the heavy ruthenium atom, for which the LANL2DZ basis set was applied to account for relativistic effects.[45] To be consistent with our previous report on [**1**]$^{3+}$,[13] we have selected the hybrid functional B3PW91 for the optimization. B3PW91 has been shown to outperform other hybrid functionals (*e.g.* B3LYP) and pure functionals (*e.g.* PW91) in numerous cases of ruthenium complexes, especially when back bonding ligands (like NO) are present.[46,47] The vibrational analyses were performed at the same level to verify that the stationary points correspond to minima on the potential energy surfaces. The UV-visible electronic spectra were then computed at the CAM-B3LYP/6-31G* level, for consistency with our previous investigation of **1**$^{3+}$.[13] This long-range corrected hybrid functional is also reported as being particularly well suited for studying molecules with very delocalized excited states.[48] Solvent effects were included by using the polarizable continuum model (PCM) implemented in Gaussian09 for acetonitrile (ε = 35.688). Molecular orbitals were plotted with GABEDIT 2.4.8.[49]

Photochemical studies

Photochemistry: Kinetic studies on the photolysis reactions were carried out with a diode array Hewlett Packard 8454 A spectrophotometer. Solutions of 2 mL of [**2**](PF$_6$)$_3$ (4.43 10^{-5} mol.L^{-1}) and [**3**](PF$_6$)$_3$ (4.48 10^{-5} mol.L^{-1}) for irradiation at 436 nm in non-deoxygenated acetonitrile were used. The optical fiber was fixed laterally from the cuvette. Absorption spectra were taken after each minute, in fast scan mode, during a period of irradiation at 436 nm of 6 hours and 4 hours for [**2**](PF$_6$)$_3$ and [**3**](PF$_6$)$_3$ respectively, which allows reaching apparent stable absorption conditions. The UV-vis spectra were recorded under irradiation realized with a Muller reactor device equipped with a cooling water filter and a mercury arc lamp equipped with appropriate interference filter to isolate the desired irradiation wavelength (λ_{max} = 436 nm). The temperature was maintained at 25 °C during the whole experiment.

Quantum yield measurements: Light intensities were determined before each photolysis experiments by chemical actinometry procedure. The actinometers used were potassium ferrioxalate and measured at λ_{irr} = 436 nm before each experiment with [**2**](PF$_6$)$_3$ and [**3**](PF$_6$)$_3$ ($I_0 = 7.0.10^{-7}$ mol.L^{-1}.s^{-1} and $8.7.10^{-7}$ mol.L^{-1}.s^{-1} respectively). The quantum yield (ϕ_A) for [**2**](PF$_6$)$_3$ and [**3**](PF$_6$)$_3$ was determined by the program Sa3.3 written by D. Lavabre and V. Pimienta.[50] It allows the resolution of the differential equation (5):

$$\frac{d[A]}{dt} = -\Phi_A\, I_a^A = -\Phi_A\, Abs_A^\lambda I_0 F \quad (5)$$

where I_a^A is the intensity of the light absorbed by the precursor; Abs_A^λ, the absorbance before irradiation; Abs_{Tot}^λ, the total absorbance; I_0, the incident intensity measured at 436 nm; and F, the photokinetic factor given by equation (6):

$$F = \frac{\left(1-10^{-Abs_{Tot}^\lambda}\right)}{Abs_{Tot}^\lambda} \quad (6)$$

The equation was fitted with the experimental data $Abs_{Tot}^\lambda = f(t)$ and 2 parameters ϕ_A and ε_B (ε_B is the molar extinction coefficient measured at the end of the reaction) at two wavelengths (λ_{irr} = 436 nm, λ_{obs} = 370 nm). λ_{obs} was chosen because it corresponds to a large difference between molar extinction coefficient at the initial and final time of the photochemical reaction. Simulation and optimization procedures were performed by using numerical integration and a non-linear minimization algorithm for the fitting of the model to the experimental data.[50,51]

For [**2**](PF$_6$)$_3$:

$[A]_0 = 4.43\ 10^{-5}$ mol. L^{-1}, $\varepsilon_A^{436} = 19639$ mol^{-1}. L. cm^{-1}, $\varepsilon_A^{370} = 17156$ mol^{-1}. L. cm^{-1}, $\varepsilon_B^{436} = 14756$ mol^{-1}. L. cm^{-1}, $\varepsilon_B^{370} = 20443$ mol^{-1}. L. cm^{-1}

For [**3**](PF$_6$)$_3$:

$[A]_0 = 4.48\ 10^{-5}$ mol. L^{-1}, $\varepsilon_A^{436} = 17411$ mol^{-1}. L. cm^{-1}, $\varepsilon_A^{370} = 18973$ mol^{-1}. L. cm^{-1}, $\varepsilon_B^{436} = 15106$ mol^{-1}. L. cm^{-1}, $\varepsilon_B^{370} = 30437$ mol^{-1}. L. cm^{-1}

Z-scan measurements

The Z-scan technique[13] was used to measure the nonlinear absorption coefficient of the samples at 800 nm using short laser pulses of 80 fs at 1 KHz of repetition rate. Molecules under study were dissolved in acetonitrile at the concentration of 1×10^{-2} mol.L^{-1}. Z-scan traces for each solution were measured at different energies (40, 62 and 100 nJ). All samples were measured at least five times for each energy. Before measuring the samples, the nonlinear transmission of the laser dye rhodamine 6G (R6G) was tested with the open aperture approach to calibrate the apparatus. In this case, the value of σ_{TPA} of R6G used to calibrate the system was the one widely accepted in the literature.[52] Then the nonlinear absorption coefficient β of each sample was obtained after fitting the normalized transmission T(z) to Z-scan formalism. The TPA cross-section (σ_{TPA}) is obtained from the following expression equation (7):

$$\sigma_{TPA} = \frac{\hbar\omega}{N}\beta \quad (7)$$

Were N is the molecular density and ω is the optical frequency.

Supporting Information (see footnote on the first page of this article): UV-vis of the ligands; DFT atomic coordinates for $\mathbf{1}^{3+}$, $\mathbf{2}^{3+}$, and $\mathbf{3}^{3+}$; comparison of coordination spheres, computed (DFT) and experimental (X-ray for $[\mathbf{1}](PF_6)_3$); NMR spectra. Photorelease from $[\mathbf{1}](PF_6)_3$; Infra-red spectra for $[\mathbf{2}](PF_6)_3$) and $[\mathbf{3}](PF_6)_3$).

Acknowledgements

The work has been performed within the framework of the French-Mexican International Laboratory (LIA-LCMMC). NF thanks CONACYT, PAIP and PAPIIP IN222819 DGAPA for financial support. VB thanks Dr. Yoichi M. A. Yamada (Riken, Center for Sustainable Resource Science, Wako, Japan) for his hospitality and facilities of his laboratory.

Conflict of Interest

The authors declare no conflict of interest.

Keywords: Ruthenium nitrosyl · Photochemistry · Two-photon absorption · Ligands design

[1] L. J. Ignarro, G. M. Buga, K. S. Wood, R. E. Byrns, G. Chaudhuri, *Proc. Natl. Acad. Sci. USA* **1987**, *84*, 9265–9269.
[2] R. M. J. Palmer, A. G. Ferrige, S. Moncada, *Nature* **1987**, *327*, 524–526.
[3] a) L. J. Ignarro, *Nitric Oxide Biology and Pathobiology*, Academic Press, San Diego, **2000**; b) B. Bonavida, *Nitric Oxide and Cancer: Prognosis, Prevention and Therapy*, Springer, New-York, **2010**; c) A. R. Butler, R. Nicholson, *Life Death and Nitric Oxide*, The Royal Society of Chemistry, Cambridge, **2003**.
[4] a) P. C. Ford, *Nitric Oxide* **2013**, *34*, 56–64; b) A. W. Carpenter, M. H. Schoenfisch, *Chem. Soc. Rev.* **2012**, *41*, 3742–3752.
[5] A. J. Burke, F. J. Sullivan, F. J. Giles, S. A. Glynn, *Carcinogenesis* **2013**, *34*, 503–512.
[6] S. Mocellin, V. Bronte, D. Nitti, *Med. Res. Rev.* **2007**, *27*, 317–352.
[7] J. C. Toledo, O. Augusto, *Chem. Res. Toxicol.* **2012**, *25*, 975–989.
[8] For recent reviews on nitric oxide delivery in biological environment, see: a) J. M. Mir, B. A. Malik, R. C. Maurya, *Rev. Inorg. Chem.* **2019**, *39*, 91–112; b) M. Paulo, L. M. Bendhack, D. E. F. R. Costa, D. Bonaventura, C. N. Lunardi, *Curr. Pharm. Des.* **2020**, *26*, 3748–3759; c) J. Cheng, Z. Shen, G. Zhang, J. Hu, K. He, Y. Yu, *Front. Chem.* **2019**, *7*, 530; d) K. T. Nguyen, Z. Wu, T. Huang, C. Y. Tay, C. Y. Tay Chor, *Curr. Med. Chem.* **2018**, *25*, 1420–1432; e) H.-J. Xiang, M. Guo, J.-G. Liu, *Eur. J. Inorg. Chem.* **2017**, *2017*, 1586–1595.
[9] a) N. L. Fry, P. K. Mascharak, *Acc. Chem. Res.* **2011**, *44*, 289–298; b) M. J. Rose, P. K. Mascharak, *Coord. Chem. Rev.* **2008**, *252*, 2093–2114.
[10] R. Santana da Silva, R. Galvao de Lima, S. P. Machado, *Adv. Inorg. Chem.* **2015**, *67*, 265–294.
[11] For recent reports on $NO^{\bullet}$ release from ruthenium nitrosyl complexes, see: a) B. Giri, S. Kumbhakar, K. K. Selvan, A. Muley, S. Maji, *New J. Chem.* **2020**, *44*, 18732–18744; b) B. Giri, T. Saini, S. Kumbhakar, K. K. Selvan, A. Muley, A. Misra, S. Maji, *Dalton Trans.* **2020**, *49*, 10772–10785; c) V. Vorobyev, D. S. Budkina, A. N. Tarnovsky, *J. Phys. Chem. Lett.* **2020**, *11*, 4639–4643; d) R. M. Motta, F. B. Santos, S. C. da Silva, G. L. C. de Souza, *Inorg. Chim. Acta* **2020**, *500*, 119202; e) I. Sasaki, S. Amabilino, S. Mallet-Ladeira, M. Tassé, A. Sournia-Saquet, P. G. Lacroix, I. Malfant, *New J. Chem.* **2019**, *43*, 11241–11250; f) M. Roose, M. Tassé, P. G. Lacroix, I. Malfant, *New J. Chem.* **2019**, *43*, 755–767; g) A. A. Mikhailov, V. A. Vorobyev, V. A. Nadolinny, Y. V. Patrushev, Y. S. Yudina, G. A. Kostin, *J. Photochem. Photobiol. A* **2019**, *373*, 37–44; h) R. Kumar, S. Kumar, M. Bala, A. Ratnam, U. P. Singh, K. Ghosh, *J. Organomet. Chem.* **2018**, *863*, 77–83; i) E. Orlowska, M. V. Babak, O. Doemoetoer, E. A. Enyedy, P. Rapta, M. Zalibera, L. Bucinsky, M. Malcek, C. Govind, V. Karunakaran, Y. Chouthury Shaik Farid, T. E. McDonnell, D. Luneau, D. Schaniel, W. Han Ang, V. B. Arion, *Inorg. Chem.* **2018**, *57*, 10702–10717; j) M. A. Crisalli, L. P. Franco, B. R. Silva, A. K. M. Holanda, L. M. Bendhack, R. S. Da Silva, P. C. Ford, *J. Coord. Chem.* **2018**, *71*, 1690–1703; k) G. A. Barbosa, J. P. da Silva, P. Appelt, O. Fuganti, F. S. Murakami, M. P. de Araujo, *Inorg. Chem. Commun.* **2018**, *90*, 108–111; l) R. Kumar, A. Yadav, A. Ratnam, S. Kumar, M. Bala, D. Sur, S. Narang, U. P. Singh, P. K. Mandal, K. Ghosh, *Eur. J. Inorg. Chem.* **2017**, *2017*, 5334–5343; m) Y. H. Li, M. Guo, S. W. Shi, Q. L. Zhang, S. P. Yang, J. G. Liu, *J. Mater. Chem. B* **2017**, *5*, 7831–7838; n) M. Guo, H. J. Xiang, Y. Wang, Q. L. Zhang, L. An, S. P. Yang, Y. Ma, Y. Wang, J. G. Liu, *Chem. Commun.* **2017**, *53*, 3253–3256.
[12] M. R. Hamblin, T. N. Demidova, *Proc. SPIE, Mechanism for Low-Light Therapy* **2006**, *6140*, 614001–614012.
[13] A. Enriquez-Cabrera, I. Sasaki, V. Bukhanko, M. Tassé, S. Mallet-Ladeira, P. G. Lacroix, R. Barba-Barba, G. Ramos-Ortiz, N. Farfán, Z. Voitenko, I. Malfant, *Eur. J. Inorg. Chem.* **2017**, *2017*, 1446–1456.
[14] Among numerous recent uses of fluorene in TPA materials, see: a) Y. Wang, Y. Wang, G. Wang, D. Liu, *J. Nonlinear Opt. Phys. Mater.* **2018**, *27*, 1850026/1–1850026/9; b) D. J. Stewart, R. Kannan, T. A. Grusenmeyer, J. M. Artz, S. L. Long, Z. Yu, T. M. Cooper, J. E. Haley, L. S. Tan, *Phys. Chem. Chem. Phys.* **2018**, *20*, 19398–19407; c) S. A. Kurhuzenkau, M. Y. Colon Gomez, K. D. Belfield, Y. O. Shaydyuk, D. J. Hagan, E. W. Van Stryland, C. Sissa, M. V. Bondar, A. Painelli, *J. Phys. Chem. C* **2018**, *122*, 5664–5672; d) L. W. Hu, L. Liang, Y. Yang, T. Guo, Y. H. Zhang, W. Yang, Y. Cao, *Chin. J. Polym. Sci.* **2018**, *36*, 546–554; e) C. Tran, N. Berqouch, H. Dhimane, G. Clermont, M. Blanchard-Desce, D. Ogden, P. I. Dalko, *Chem. Eur. J.* **2017**, *23*, 1860–1868; f) M. G. Vivas, R. D. Fonseca, J. P. Siqueira, C. R. Mendonca, P. C. Rodrigues, L. De Boni, *Materials* **2017**, *10*, 512/1–512/11; g) J. B. Verlhac, G. Clermont, M. Blanchard-Desce, *J. Porphyr. Phtalocyanines* **2017**, *21*, 77–87; h) R. Liu, M. Shu, J. Hu, S. Zhu, H. Shi, H. Zhu, *Dyes Pigm.* **2017**, *137*, 174–181.
[15] M. Pawlicki, H. A. Collins, R. G. Denning, H. L. Anderson, *Angew. Chem. Int. Ed.* **2009**, *48*, 3244–3266; *Angew. Chem.* **2009**, *121*, 3292–3316.
[16] B. Strehmel, V. Strehmel, in: *Advances in Photochemistry* (Eds.: D. C. Neckers, W. S. Jenks, T. Wolff), J. Wiley & Sons, Inc. **2007**, Vol. 29, pp. 111–341.
[17] P. V. Simpson, L. A. Watson, A. Barlow, G. Wang, M. P. Cifuentes, M. G. Humphrey, *Angew. Chem. Int. Ed.* **2016**, *55*, 2387–2391; *Angew. Chem.* **2016**, *128*, 2433–2437.
[18] C. Andraud, R. Fortrie, C. Barsu, O. Stéphan, H. Chermette, P. L. Baldeck, *Adv. Polym. Sci.* **2008**, *214*, 149–203.
[19] W. Zhang, X. Y. Cao, Y. Zi, J. Pei, *Org. Lett.* **2005**, *7*, 959–962.
[20] E. C. Constable, M. D. Ward, *J. Chem. Soc. Dalton Trans.* **1990**, 1405–1409.
[21] K. T. Potts, D. Konwar, *J. Org. Chem.* **1991**, *56*, 4815–4816.
[22] V. Bukhanko, P. G. Lacroix, I. Sasaki, M. Tassé, Z. Voitenko, I. Malfant, *Inorg. Chim. Acta* **2018**, *482*, 195–205.
[23] H. M. Kim, B. R. Cho, *Chem. Commun.* **2009**, 153–154.
[24] F. Terenziani, C. Katan, E. Badaeva, S. Tretiak, M. Blanchard-Desce, *Adv. Mater.* **2008**, *20*, 4641–4678.
[25] A. D. Laurent, D. Jacquemin, *Int. J. Quantum Chem.* **2013**, *113*, 2019–2039.
[26] J. Akl, I. Sasaki, P. G. Lacroix, I. Malfant, S. Mallet-Ladeira, P. Vicendo, N. Farfán, R. Santillan *Dalton Trans.* **2014**, *43*, 12721–12733.
[27] A. Enriquez-Cabrera, P. G. Lacroix, I. Sasaki, S. Malet-Ladeira, N. Farfan, R. M. Barba-Barba, G. Ramos-Ortiz, I. Malfant, *Eur. J. Inorg. Chem.* **2018**, *2017*, 531–543.
[28] M. Roose, I. Sasaki, V. Bukhanko, S. Mallet-Ladeira, R. M. Barba-Barba, G. Ramos-Ortiz, A. Enriquez-Cabrera, N. Farfán, P. G. Lacroix, I. Malfant, *Polyhedron* **2018**, *151*, 100–111.
[29] S. Amabilino, M. Tasse, P. G. Lacroix, S. Mallet-Ladeira, V. Pimienta, J. Akl, I. Sasaki, I. Malfant New, *J. Chem.* **2017**, *41*, 7371–7383.
[30] A. F. Vanin, A. P. Poltorakov, V. D. Mikoyan, L. N. Kubrina, E. van Faassen, *Nitric Oxide* **2006**, *15*, 295–311.
[31] A. J. Liu, Q. Duan, J. Wang, Z. Song, X. Qiao, H. Wang, *J. Biomed. Opt.* **2015**, *20*, 015004-1–015004-7.
[32] J. Akl, I. Sasaki, P. G. Lacroix, V. Hugues, P. Vivendo, M. Bocé, S. Mallet-Ladeira, M. Blanchard-Desce, I. Malfant, *Photochem. Photobiol.* **2016**, *15*, 1484–1491.

[33] E. W. Van Stryland, M. Sheik-Bahae, in: *Characterization Techniques and Tabulations for Organic Nonlinear Material*s (Eds.: M. G. Kuzyk, C. W. Dirk), Marcel Dekker, Inc., **1998**, p.655–682.
[34] J. O. Morley, *Int. J. Quantum Chem.* **1993**, *46*, 19–26.
[35] O. Mongin, L. Porrès, M. Charlot, C. Katan, M. Blanchard-Desce, *Chem. Eur. J.* **2007**, *13*, 1481–1498.
[36] M. Drobizhev, F. Meng, A. Rebane, Y. Stepanenko, E. Nickel, C. W. Spangler, *J. Phys. Chem. B* **2006**, *110*, 9802–9814.
[37] M. Albota, D. Beljonne, J. L. Brédas, J. E. Ehrich, J. Y. Fu, A. A. Heikal, S. E. Hess, T. Kogej, M. D. Levin, S. R. Marder, D. MacCord-Maughon, J. W. Perry, H. Röckel, M. Rumi, G. Subbramaniam, W. W. Webb, X. L. Wu, C. Xu, *Science* **1998**, *281*, 1653–1656.
[38] B. J. Orr, J. F. Ward, *Mol. Phys.* **1971**, *20*, 513–526.
[39] Y. Chitose, M. Abe, K. Furukawa, C. Katan, *Chem. Lett.* **2016**, *45*, 1186–1188.
[40] L. Ventelon, S. Charier, L. Moreaux, J. Mertz, M. Blanchard-Desce, *Angew. Chem. Int. Ed.* **2001**, *40*, 2098–2101; *Angew. Chem.* **2001**, *113*, 2156–2159.
[41] M. Drobizhev, Y. Stepanenko, Y. Dzenis, A. Karotki, A. Rebane, P. N. Taylor, H. L. Anderson, *J. Phys. Chem. B* **2005**, *109*, 7223–7236.
[42] M. -C Yoon, S. B. Noh, A. Tsuda, Y. Nakamura, A. Osuka, D. Kim, *J. Am. Chem. Soc.* **2007**, *129*, 10080–10081.
[43] M. Romero-Ávila, A. F. León Rojas, P. G. Lacroix, I. Malfant, N. Farfan, R. Mhanna, R. Santillan, G. Ramos-Ortiz, J.-P. Malval, *J. Phys. Chem. Lett.* **2020**, *11*, 6487–6491.
[44] Gaussian 09, Revision E.01, M. J. Frisch, G. W. Trucks, H. B. Schlegel, G. E. Scuseria, M. A. Robb, J. R. Cheeseman, G. Scalmani, V. Barone, B. Mennucci, G. A. Petersson, H. Nakatsuji, M. Caricato, X. Li, H. P. Hratchian, A. F. Izmaylov, J. Bloino, G. Zheng, J. L. Sonnenberg, M. Hada, M. Ehara, K. Toyota, R. Fukuda, J. Hasegawa, M. Ishida, T. Nakajima, Y. Honda, O. Kitao, H. Nakai, T. Vreven, J. A. Montgomery, Jr., J. E. Peralta, F. Ogliaro, M. Bearpark, J. J. Heyd, E. Brothers, K. N. Kudin, V. N. Staroverov, R. Kobayashi, J. Normand, K. Raghavachari, A. Rendell, J. C. Burant, S. S. Iyengar, J. Tomasi, M. Cossi, N. Rega, J. M. Millam, M. Klene, J. E. Knox, J. B. Cross, V. Bakken, C. Adamo, J. Jaramillo, R. Gomperts, R. E. Stratmann, O. Yazyev, A. J. Austin, R. Cammi, C. Pomelli, J. W. Ochterski, R. L. Martin, K. Morokuma, V. G. Zakrzewski, G. A. Voth, P. Salvador, J. J. Dannenberg, S. Dapprich, A. D. Daniels, Ö. Farkas, J. B. Foresman, J. V. Ortiz, J. Cioslowski, D. J. Fox, Gaussian, Inc., Wallingford CT, 2009.
[45] a) P. J. Hay, W. R. Wadt, *J. Chem. Phys.* **1985**, *82*, 270–283; b) W. R. Wadt, P. J. Hay, *J. Chem. Phys.* **1985**, *82*, 284–298; c) P. J. Hay, W. R. Wadt, *J. Chem. Phys.* **1985**, *82*, 299–310.
[46] M. J. Rose, P. K. Mascharak, *Inorg. Chem.* **2009**, *48*, 6904–6917.
[47] P. Hirva, M. Haukka, M. Jaconen, *J. Mol. Model.* **2008**, *14*, 171–181.
[48] D. Jacquemin, E. A. Perpète, G. E. Scuseria, I. Ciofini, C. Adamo, *J. Chem. Theory Comput.* **2008**, *4*, 123–135.
[49] http://sites.Google.com/site/allouchear/Home/gabedit.
[50] Program Sa3.3 written by D. Lavabre and V. Pimienta (http://cinet.ch-im.pagesperso-orange.fr/tele sa/install Sa.html).
[51] V. Pimienta, C. Frouté, M.-H. Deniel, D. Lavabre, R. Guglielmetti, J.-C. Micheau, *J. Photochem. Photobiol. A* **1999**, *122* 199–204 (reference 35).
[52] N. S. Makarov, M. Drobizhev, A. Rebane, *Opt. Express* **2008**, *16*, 4029–4047.

Manuscript received: February 8, 2021
Revised manuscript received: March 15, 2021